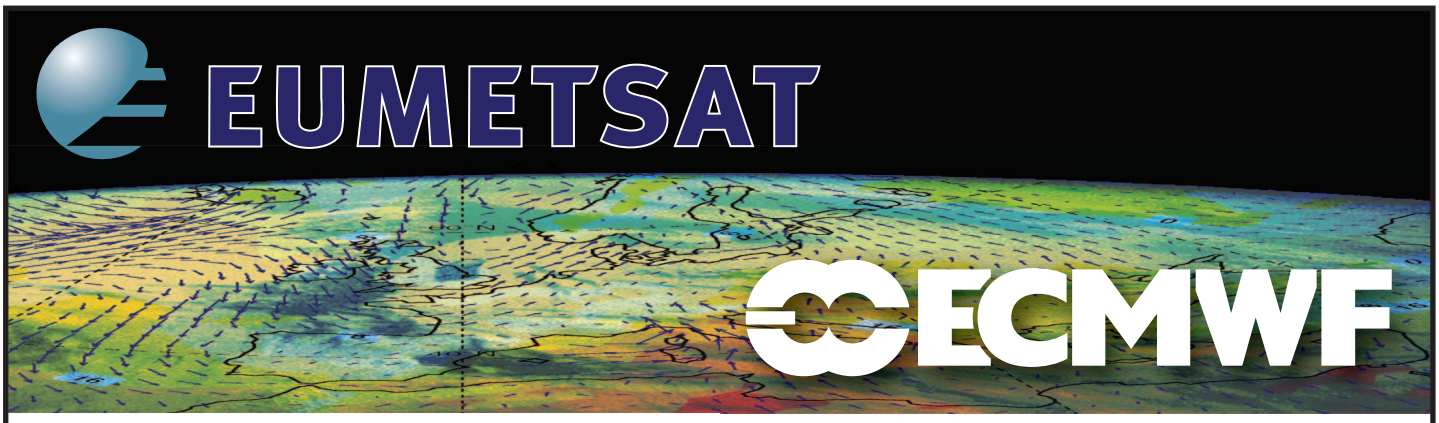

EUMETSAT/ECMWF Fellowship Programme
Research Report No. 27

SSMI/S radiances over land in the all-sky framework: one year report

F. Baordo, A. J. Geer and S. English

November 2012

Series: EUMETSAT/ECMWF Fellowship Programme Research Reports

A full list of ECMWF Publications can be found on our web site under:
http://www.ecmwf.int/publications/

Contact: library@ecmwf.int

European Centre for Medium Range Weather Forecasts
Shinfield Park, Reading, RG2 9AX, England

Abstract

Microwave satellite data over land are still not as intensively used in numerical weather prediction (NWP) as are observations over ocean. Land surface variability in space and time (vegetation, soil moisture, roughness, snow and ice) makes skin temperature and emissivity two parameters difficult to estimate and, as a consequence, simulations of brightness temperature are not as good over land as over ocean. Some feasibility studies have been conducted to investigate the possibility of assimilating SSMI/S humidity sounding channels over land within the ECMWF system in the all-sky framework. New developments have been made in order to have land surface emissivity estimations available at the frequencies proposed for the assimilation. Land emissivity retrieval was implemented within the scattering radiative transfer code (RTTOV-SCATT) so that the emissivity retrieved takes into account cloud and precipitation. SSMI/S and AMSU-A window channel retrievals, assessed by comparison to independent emissivity data, show that emissivity estimates are feasible in the all-sky approach. The findings also show that at higher microwave frequencies (greater than 85 GHz), independently of the sensor, observation geometry and the scheme implemented (clear-sky or all-sky), the emissivity estimation is more affected by cloud contamination and consequently it might lead to retrievals which must be rejected.

Land emissivity retrieved from SSMI/S window channel 18 was given to the humidity sounding channels (channel 9, 10 and 11) and, subsequently, first guess departures were computed by running assimilation experiments, using the incremental 4D-Var ECMWF system at T255 horizontal resolution, from August to October 2011. The initial sample of SSMI/S humidity sounding observations over land was characterised by large positive and negative first guess departures with negative values greater than -40 K. At high microwave frequencies, the Mie soft sphere approximation used to simulate the scattering properties of ice and snow particles is not accurate enough leading to warmer modelled radiances than observed. Aside from deficiencies in RTTOV-SCATT calculations, the non-Gaussian behaviour of first guess departures is also affected by mislocation errors, in other words, the forecast model might not be good at predicting cloud, precipitation and surface conditions with exactly the right intensity and location. A screening methodology was investigated in order to reduce these inconsistencies. The results show that the use of a scattering index (SI) quality check is necessary to detect observations affected by ice hydrometeor scattering process and reduce most of the inconsistencies between observed and modelled radiances. In fact, the SI screening rejects about 32% of the initial observations, whilst only $6-7\%$ of observations are rejected by two additional quality checks that were used to remove residual inconsistencies. The use of the SI defined as SSMI/S brightness temperatures difference at channel 17 and channel 8 was found to be the best screening methodology.

The screening strategy applied to the initial sample of data over land is able to detect a sub-set of observations, in each humidity sounding channel, which are strongly correlated to the corresponding simulated radiances with correlation coefficients larger than 0.95 and root mean square differences between the observed and modelled brightness temperatures lower than 1.70 K. In addition, the resultant SSMI/S PDFs of first guess departures show a good Gaussianity. The PDFs were also compared to those provided by MHS observations actively assimilated over land in clear-sky conditions within the ECMWF system. The findings show that first guess departures of SSMI/S and MHS humidity sounding channels not only have very similar distribution in shape and intensity, but the standard deviations computed over the whole sample are also comparable. This result is very important as a Gaussian and unbiased distribution of first guess departure is the necessary 4D-Var assumption that must be satisfied before any sample of observations can be considered for an assimilation experiment. Additionally, at 183.31 ± 1.0 GHz, the residual cloud contamination, which the SSMI/S screening methodology might reasonably take into account, seems to be correctly managed by the all-sky framework, while remaining negative first guess departures biases are still observed in the MHS sample of assimilated observations.

1 Introduction

Satellite radiance observations are increasingly being assimilated into operational NWP systems in cloudy and precipitating areas. At ECMWF, the all-sky approach is implemented to operationally assimilate microwave imagers (SSMI/S F17, TMI and AMSR-E, before the antenna fault in October 2011) and to monitor passively AMSU-A channel 4 and 5 over ocean (Bauer et al. 2010, Geer et al. 2010, 2011, 2012). In the all-sky scheme clear, cloudy and precipitating scenes are treated in the same stream, including scattering radiative transfer where necessary. This gives a wider observational coverage and brings information on water vapour, cloud and precipitation into the analysis, benefitting forecasts. It is worth studying whether the all-sky approach can be extended over land and the SSMI/S humidity sounding channels (183.31 $\pm$ 6.6, 183.31 $\pm$ 3.0 and 183.31 $\pm$ 1.0 GHz, horizontal polarization) have been selected for the aim of this study. The use of these channels might bring additional and complementary information to that already available by the assimilation of other microwave sounders radiances and helps to enhance and constrain the humidity analysis. So far, the use of microwave observations from temperature and humidity sounding channels is still more intensive over ocean than over land. Their use over land is still limited to channels that receive a weak contribution from the surface. This limitation is less important over oceans: seas are associated with low emissivity values and high emissivity polarisation differences and emissivity models have been developed that are accurate enough to meet the NWP requirements. On the contrary, land surface emissivity at microwave frequencies are rather high and vary in a complex way with surface type, roughness and moisture among other parameters. For these reasons, the use of radiances over land in the all-sky framework has not yet been thoroughly examined and an accurate investigation is necessary before any assimilation experiment can be considered. Hence, the goal of this work is to provide a feasibility study on the possibility of achieving the assimilation of SSMI/S humidity sounding channels over land in the all-sky framework.

Land surface emissivity estimations must be available in the all-sky framework in order to investigate differences between observed and simulated radiances at the frequencies proposed for this study. Estimation of land surface emissivity is a well known problem in literature due to its high temporal and spatial variability and has been investigated by many authors. Among the methods to retrieve land surface emissivity, many have previously adopted satellite observations in order to have an analytical emissivity estimate (English et al. 1998, Karbou et al. 2005, 2007, Prigent et al. 1997, 2005). Such a retrieval scheme has been developed in the ECMWF assimilation system for all the sensors available within the all-sky framework and is applied to those channels which have surface sensitivity (window channels). The implementation of the emissivity retrieval has been coded within the scattering radiative transfer code (RTTOV-SCATT) so that the emissivity retrieved takes into account cloud and precipitation.

In order to investigate the feasibility of assimilating SSMI/S radiances over land, land emissivity retrieved from 91 GHz, horizontal polarization, has been given to the humidity sounding channels and used to compute radiative transfer calculations to obtain simulated radiances. Differences between observations and simulated brightness temperatures (so called first guess departures) were obtained by running assimilation experiments, using the incremental 4D-Var ECMWF system at T255 horizontal resolution ($\sim$78 km), from August to October 2011. SSMI/S humidity sounding first guess departures were analysed to study the differences between modelled and observational information and to define the best screening strategy to select those observations which might be considered plausible for an assimilation experiment. MHS observations actively assimilated over land in a clear-sky approach within the ECMWF system were also used as a reference to validate the screening methodology implemented.

This report is presented as follows. Section 2 summarises the technical implementation and verification of the emissivity retrieval in the all-sky framework: section 2.2 describes how the implementation was

coded; sections 2.3 and 2.4 show, respectively, the results of the land surface emissivity estimates using SSMI/S and AMSU-A data. Section 3 describes the methodology adopted to select those SSMI/S humidity sounding observations which might be taken into account for an assimilation experiment: section 3.2 summaries the screening strategy investigated, whilst in section 3.3, SSMI/S data selected using the screening methodology are compared with MHS observations actively assimilated within the ECMWF system. General summary and conclusions are discussed at the end of the report.

2 The emissivity retrieval in the all-sky framework

2.1 Data

The SSMI/S sensor (Kunkee et al. 2008) represents an important advancement over its predecessor, SSM/I, as it combines the SSM/I imaging capabilities with the profiling capabilities of microwave sounders. SSMI/S allows microwave measurements at 24 frequencies ranging from 19 to 183 GHz, and has 14 channels in the 50-60 GHz range which allow atmospheric temperature sensing from about 80 km down to the earth surface. In addition to temperature sounding channels, SSMI/S combines humidity sounding channels close to the strong 183 GHz water vapour line as well as imaging channels in common with SSM/I. SSMI/S observations used in this study are pre-processed according to the strategy developed by Bell et al. (2008): solar intrusion affected data is excluded and a correction is applied for the thermal emissions from the instruments reflector.
AMSU-A and MHS sounders have been operating on board the latest generation of the National Oceanic and Atmospheric Administration (NOAA) polar orbiting satellites since May 1998. AMSU-A is designed for atmospheric temperature sensing whereas the MHS sounder is used for humidity probing. The AMSU-A instrument makes measurements at 15 frequencies which include 12 frequencies near the oxygen absorption band (50-60 GHz). MHS makes measurements at 3 frequencies close to the strong water vapour absorption line at 183.31 GHz. In addition to sounding channels, AMSU-A and MHS have the so-called window channels which give measurements sensitive to the surface and to low level atmospheric layers (23.8, 31.4, 50.3, 89, and 150 GHz). Both instruments observe the Earth with a scan angle that varies from -48° to 48° with respect to nadir.

2.2 Implementation of the emissivity retrieval in the all-sky framework

The surface emissivity is a parameter directly involved in the radiative transfer calculations to compute the simulated brightness temperatures. An emissivity estimate as close as possible in time and space to the observation is beneficial. Hence, the first step towards the SSMI/S data assimilation over land is to ensure an emissivity scheme is available in the all-sky framework.

For a specular surface and for a given zenith (θ) angle and frequency (ν), the brightness temperature (T_b) observed by the sensor can be expressed as:

$$T_b(\theta,\nu) = T_s\varepsilon(\theta,\nu)\Gamma + (1-\varepsilon(\theta,\nu))\Gamma T^{\downarrow}(\theta,\nu) + T^{\uparrow}(\theta,\nu), \quad (1)$$

where $\varepsilon(\theta,\nu)$ represent the surface emissivity at frequency ν and at observation zenith angle θ. T_s, $T^{\downarrow}(\theta,\nu)$ and $T^{\uparrow}(\theta,\nu)$ are the surface skin temperature, the atmospheric down-welling and up-welling

radiation respectively. Γ is the net atmospheric transmissivity and can be expressed as a function of the atmospheric opacity τ(0,H) and the observation zenith angle θ, where H is the top of atmosphere height:

$$\Gamma = exp\left(\frac{-\tau(0,H)}{cos(\theta)}\right). \tag{2}$$

The emissivity can be retrieved from equation 1 as follows:

$$\varepsilon(\theta,\nu) = \frac{T_b(\theta,\nu) - T^{\uparrow}(\theta,\nu) - T^{\downarrow}(\theta,\nu)\Gamma}{(T_s - T^{\downarrow}(\theta,\nu))\Gamma}. \tag{3}$$

Short-range forecast data (such as temperature and humidity profiles) are used as inputs to the radiative transfer model in order to calculate the atmospheric contribution to the measured T_b ($T^{\downarrow}(\theta,\nu)$, $T^{\uparrow}(\theta,\nu)$ and Γ). The land surface skin temperature T_s is taken from the short-range forecasts as well. As already mentioned, land surface skin temperatures are also affected by spatial and temporal variability and, as a result, T_s estimates obtained by NWP modeling and assimilation systems might be biased. In this report, we did not investigate the use of different land surface skin temperature sources (such as pre-calculated monthly mean climatology or retrieved by instantaneous measures of microwave brightness temperature), but the impact of T_s on the emissivity retrieval might be considered in the future as an additional study.

Equation 3 represents the scheme that is generally used within NWP systems to retrieve emissivity from satellite observations for those channels that receive strong contribution from the surface (the so-called window channels). The derived emissivity is assigned afterwards to temperature or humidity sounding channels. This is also used at ECMWF, where AMSU-A and MHS data are operationally assimilated over land in clear-sky conditions. For instance, emissivity derived from AMSU-A channel 3 (50.3 GHz) is given to temperature channels, whilst retrievals from MHS channel 1 (89 GHz) are performed to assign emissivity to humidity channels.

In the all-sky framework the observation operator is RTTOV-SCATT (Bauer et al. 2006), which provides scattering radiative transfer calculations at microwave frequencies. Scattering properties are pre-calculated using Mie theory and tabulated as function of frequencies, temperature and hydrometer type and density. The most important inputs to RTTOV-SCATT are the surface skin temperature and winds, and vertical profiles of pressure, temperature, moisture, cloud liquid water and ice, rain and frozen precipitation fluxes and cloud cover. RTTOV-SCATT calculates the all-sky simulated or first guess brightness temperature (T_{fg}), which depends on the overall cloud fraction C (Geer et al. 2009) as follows:

$$T_{fg} = (1-C)T_{clr} + CT_{cld}. \tag{4}$$

T_{clr} and T_{cld} are the simulated brightness temperatures of a clear column, taking into account only gaseous absorption, and a cloudy column, taking into account cloud, precipitation and scattering. C, the cloud fraction over the whole profile, depends not only on the hydrometeor amount (cloud liquid, cloud ice, rain and snow densities) but also on the convective and large-scale precipitation fractions at each layer of the atmosphere. The necessary inputs to compute C are taken separately from the outputs of the convective and large-scale moist physics parametrizations. For computational reasons, for model profiles where

C is greater than 0.05, the equivalent observation in model space is computed according to equation 4, otherwise the simulated brightness temperature is calculated considering only the clear column, in other words $T_{fg} = T_{clr}$.

Consistent with the radiance computation, the emissivity retrieval in the all-sky approach has been implemented considering equation 3 where C is less than or equal to 0.05, otherwise the contribution from clear and cloudy column is taken into account as follows:

$$\varepsilon(\theta,\nu) = \frac{T_b(\theta,\nu) - (1-C)T^{\uparrow}_{clr}(\theta,\nu) - (1-C)T^{\downarrow}_{clr}(\theta,\nu)\Gamma_{clr} - CT^{\uparrow}_{cld}(\theta,\nu) - CT^{\downarrow}_{cld}(\theta,\nu)\Gamma_{cld}}{(1-C)(T_s - T^{\downarrow}_{clr}(\theta,\nu))\Gamma_{clr} + C(T_s - T^{\downarrow}_{cld}(\theta,\nu))\Gamma_{cld}}, \quad (5)$$

where $T^{\downarrow}_{clr}(\theta,\nu)$, $T^{\uparrow}_{clr}(\theta,\nu)$, Γ_{clr} are the atmospheric down-welling and up-welling radiation and the atmospheric transmissivity of the clear column and $T^{\downarrow}_{cld}(\theta,\nu)$, $T^{\uparrow}_{cld}(\theta,\nu)$, Γ_{cld} are the same quantities but for the cloudy column. Equation 5 is reduced to equation 3 when C = 0.

In conclusion, independently of the satellite observation available (SSMI/S, TMI or AMSU-A), the all-sky framework implements emissivity and first guess radiance computations as follows:

a. where C $\leq$ 0.05: $T_{fg} = T_{clr}$ and ε according to equation 3,

b. where C $>$ 0.05: T_{fg} = (1-C)T_{clr} + CT_{cld} and ε according to equation 5.

Assumption a and b are, respectively, the clear-sky and the cloudy-sky calculations embedded in the all-sky framework for computational reasons. For the satellite radiances not assimilated in the all-sky framework, but in other schemes through the IFS code, the clear-sky implementation is used only: C is not taken into account, ε is estimated according to equation 3 and the modelled brightness temperature is computed ignoring the effect of the hydrometeors ($T_{fg} = T_{clr}$).

In the following sections, the technical verification of the emissivity retrieval implemented in the all-sky framework (assumption a and b) is verified with independent data. SSMI/S F17 surface emissivity estimations in the clear-sky assumption a (using equation 3) were compared with data provided by a Tool to Estimate Land Surface Emissivities at Microwave frequencies (TELSEM, Aires et al. 2010), a package available within RTTOV (RTTOV v10), where pre-calculated monthly mean emissivity climatology derived from ten-year SSM/I observations are stored (section 2.3). The impact on the emissivity computation introduced by the cloud-precipitation correction term in equation 5 (cloudy-sky assumption b) was evaluated by comparing AMSU-A estimations with AMSU-A retrievals obtained by a completely independent clear-sky implementation available within another path of the IFS code (section 2.4).

2.3 Technical verification of the clear-sky emissivity retrieval in the all-sky framework

The purpose of this section is to verify the implementation of the emissivity retrieval within the all-sky framework when the clear-sky assumption is used (equation 3). In this context, SSMI/S F17 observations were selected where the cloud fraction C is less than 0.05. No additional quality controls were applied. The sub-set of SSMI/S observations obtained were used to retrieve land surface emissivities that were compared with emissivity estimates provided by TELSEM. As already mentioned, TELSEM is based on a pre-calculated monthly-mean emissivity climatology derived from Special Sensor Microwave/Imager

	R (%)				RMS			
Freq (GHz)	G	NH	T	SH	G	NH	T	SH
19h	89	91	86	77	0.022	0.021	0.022	0.025
19v	63	62	59	62	0.017	0.018	0.015	0.016
37h	91	92	87	78	0.020	0.020	0.019	0.023
37v	70	70	63	69	0.020	0.021	0.016	0.019
91h	78	83	58	73	0.027	0.025	0.036	0.021
91v	57	63	29	68	0.025	0.025	0.032	0.019

Table 1: Pearson correlation (R) coefficients and root mean square (RMS) differences for SSMI/S and TELSEM emissivity estimations. Calculations for each SSM/I-like window frequency were conducted globally [60,-60], G, Northern hemisphere [60,20], NH, Tropics [20,-20], T, and Southern hemisphere [-20,-60], SH. The sample of observations is from 1 to 31 August 2011.

(SSM/I) observations and provides emissivity estimates and error-covariance matrices for land surfaces at any latitude between 19 and 100 GHz and for all angles and linear polarization.

Agreement between SSMI/S and TELSEM emissivity calculations was examined for the SSM/I-like window channels: 19.35 GHz, 37 GHz and 91.655 GHz for both horizontal and vertical polarizations (channel 12 to channel 18). For each SSMI/S frequency, the corresponding emissivity retrievals were compared with TELSEM estimations by means of scatter and histogram plots and mean emissivity maps. Verifications were performed globally for latitudes ranging from -60 to 60 degrees and for the Northern hemisphere (60,20), Tropics (20,-20) and Southern hemisphere (-20,-60). The latitude range was chosen to match the all-sky assimilation coverage over ocean and also to avoid the higher latitudes where the retrieval error might be larger due to snow and ice surfaces. The sample of observations considered is 1 month of data (1 to 31 August 2011). To give a statistical measure of the two different emissivity computations, root mean square (RMS) differences between SSMI/S and TELSEM emissivity estimations and Pearson correlation (R) coefficients were also computed. RMS and R are summarised in table 1 for each SSM/I-like frequency and geographical area.

In each geographical area, SSMI/S emissivity retrievals at horizontal polarization (19h, 37h and 91h) show the highest correlation to emissivity estimations provided by TELSEM. In contrast, vertical polarization (19v, 37v and 91v) seems to exhibit slightly lower RMS differences values. This is a very good result considering that emissivity derived from satellite observations is directly affected by space and time variability of parameters such as soil moisture, standing water or snow and topographic roughness, which are all surface characteristics that interact with the microwave radiation depending upon frequency, incidence angle and polarization. It is reasonable that emissivities analytically retrieved by satellite observations show slight diversity with respect to monthly-mean climatologies of emissivities. The general good agreement between SSMI/S retrievals and TELSEM estimates demonstrates the consistency of SSMI/S window channels emissivity calculations implemented within the all-sky framework. For simplicity, in this report we present plots and maps for the higher microwave window frequencies (91h and 91v) only. It is worth analysing more in detail the emissivity estimations at 91 GHz because emissivity retrieved from channel 18 (91h) was assigned to the humidity sounding channels in order to investigate the feasibility of assimilating SSMI/S radiances over land.

Emissivity maps (figure 1 and 2) show the expected variations with polarization and surface types: desert areas (for instance Northern Africa and the Arabian Peninsula) are associated with lower emissivity values for horizontal polarization than in surrounding vegetated areas. On the contrary, densely vegetated zones, such as the tropical rainforest in Africa or in South America, where vegetation absorbs, emits and

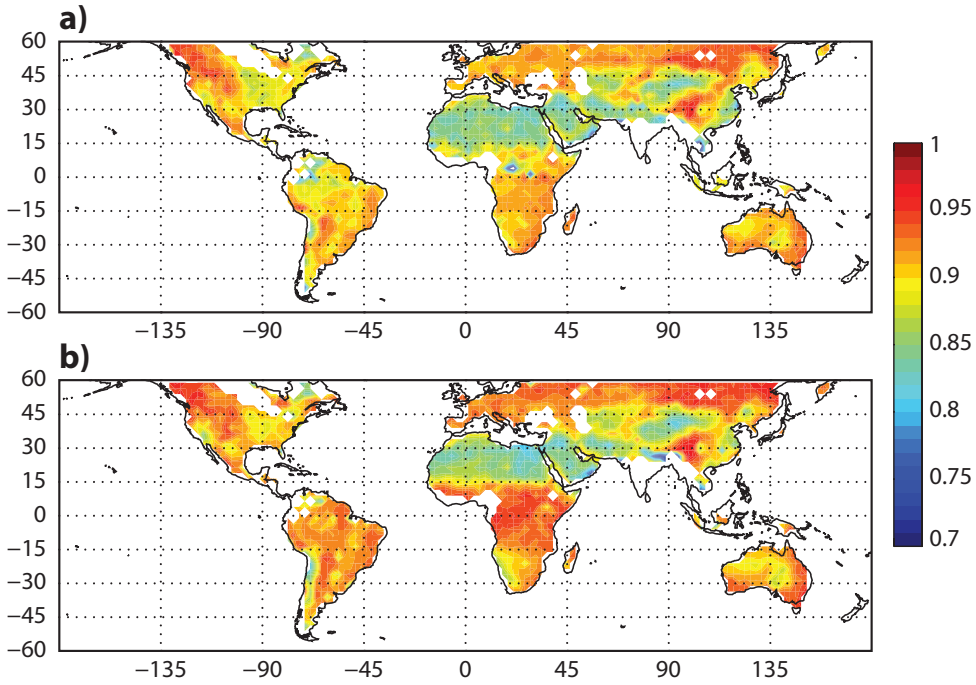

Figure 1: Mean land emissivity maps of SSMI/S channel 18 (91h) retrievals, a, and TELSEM estimations, b. Maps are binned in 2.5 by 2.5 boxes over 1 month of data (1-31 August 2011).

scatters microwave radiation, exhibit high emissivity for horizontal polarization and reduce differences with vertical polarization. Scatter and histogram plots (figure 3 and 4) of SSMI/S emissivity retrievals and TELSEM emissivity estimations are also in good agreement. However, a number of retrievals at both 91h and 91v are characterised by low emissivity estimates, values which are not likely to be true. These values can be easily seen in the scatter plots and localised in the emissivity maps over Central Africa (blue spots in figure 1 and 2). This might happen as calculations at these high microwave frequencies are affected by large variability related to water-vapour and cloud contamination producing unreliable emissivity estimations. The points characterised by low emissivity estimates seem not have any particular dependency on high orography (it ranges from 0 to 500 m), skin surface temperature (it ranges from 290 to 300 K) or observation time (day or night time). On the contrary, observed radiances at 91h and 91v are affected by larger brightness temperature depression than the other window channels. One of these SSMI/S observations is analysed more in detail in table 2.

Brightness temperatures at 91h and 91v are about 50 K colder than the radiances observed at 19h and 19v. On the contrary, depressions observed at 37 GHz are not larger than 21 K. As a consequence, emissivity retrievals at 19h and 19v, frequencies not affected by cloud contamination, are in agreement with those provide by TELSEM estimations. Moving at higher frequencies, retrievals at 37 GHz are still reasonable, but slightly contaminated by cloud influence, whilst at 91 GHz estimations are completely affected by cloud contamination producing implausible land surface emissivities. It will be a matter of quality control to screen out such observations.

2.4 Technical verification of the cloudy-sky emissivity retrieval in the all-sky framework

The aim of this section is to verify the technical implementation of the emissivity retrieval in the all-sky framework, when the cloud-precipitation correction term is taken into account (cloudy-sky assumption,

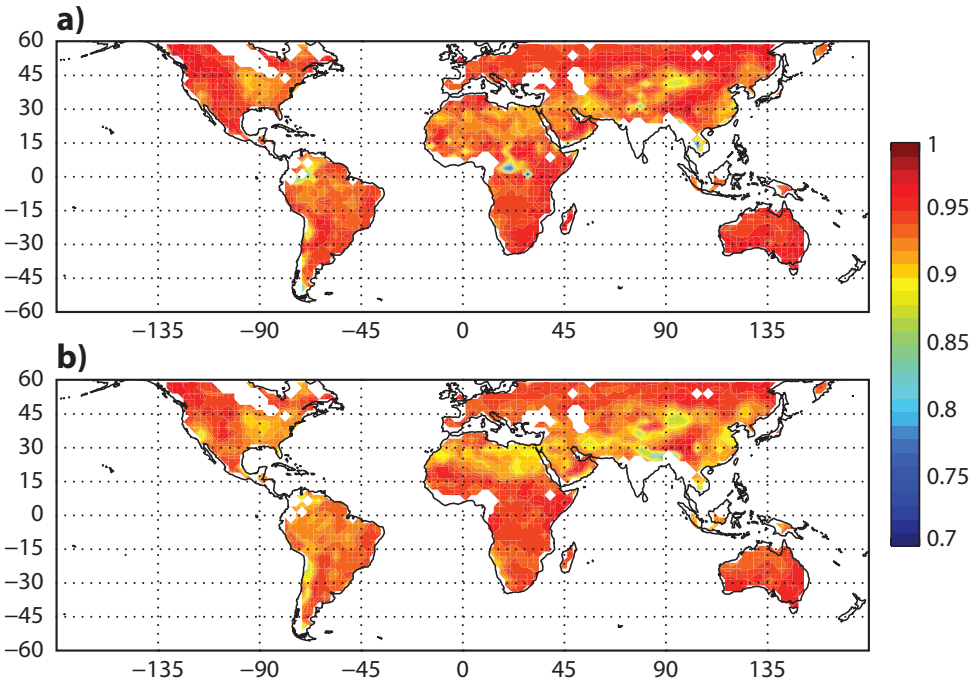

Figure 2: As figure 1, but for SSMI/S channel 17 (91v).

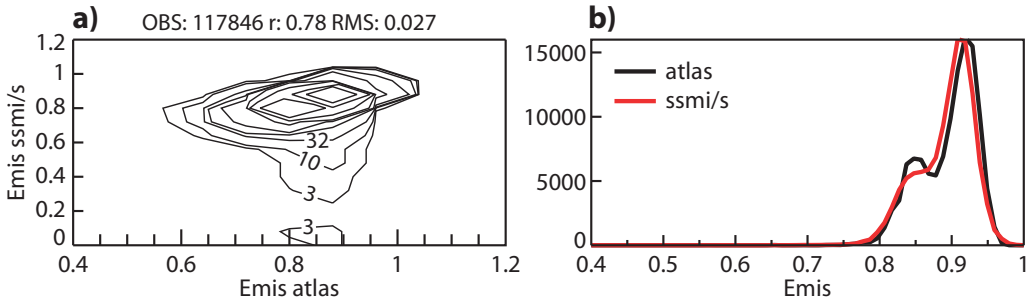

Figure 3: Scatter plot, a, and histogram, b, of SSMI/S channel 18 (91h) emissivity retrievals versus TELSEM emissivity estimations (captioned as atlas). The sample of observations is 1 month of data (1-31 August 2011) and latitude ranges from -60 to 60 degrees. The scatter plot density is represented by logarithmic contours at 3, 10, 32, 100 and so on, per 0.08 by 0.08 bin. Number of observations (OBS), Pearson correlation coefficients (r) and root mean square (RMS) differences are also shown. Histogram bin size is 0.01.

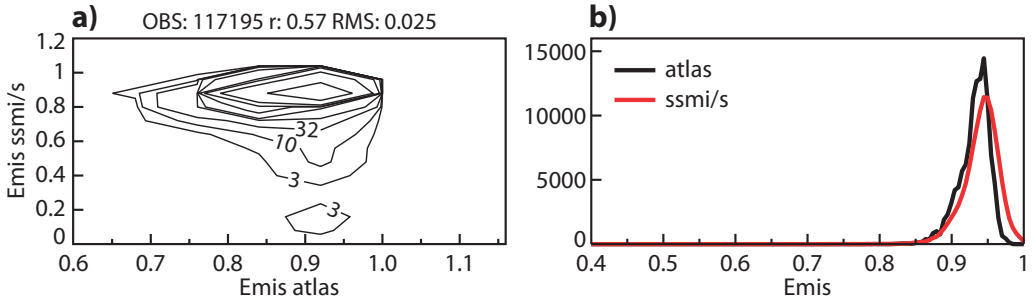

Figure 4: As figure 3, but for SSMI/S channel 17 (91v).

latitude	3.93					
longitude	21.38					
observation time	04:14:41					
skin surface temperature (K)	293.59					
orography (m)	484.42					
SSMI/S channel	19h	19v	37h	37v	91h	91v
observed radiance (K)	283.42	281.73	262.47	263.77	233.22	229.99
emissivity retrieval	0.9421	0.9364	0.8490	0.8549	0.2288	0.1595
TELSEM estimation	0.9607	0.9643	0.9418	0.9434	0.9464	0.9464
TELSEM STD	0.0150	0.0139	0.0404	0.0144	0.0142	0.0435

Table 2: SSMI/S observation characterised by low emissivity estimates at 91h and 91v.

equation 5). AMSU-A observations are used in this case. As already mentioned, beside microwave imager data, the all-sky approach passively monitors AMSU-A channel 4 and 5, in other words, AMSU-A observations are available to compute emissivity retrievals in the all-sky framework. According to the assumption in the all-sky framework, the cloudy-sky emissivity retrieval was applied to those AMSU-A observations where the cloud fraction C is greater than 0.05. In this section, the cloudy-sky emissivity retrievals are simply referred as all-sky retrievals. AMSU-A observations are also operationally assimilated in a completely independent path through the IFS code. In this framework, AMSU-A data over land are assimilated in clear-sky conditions only and an independent emissivity retrieval is implemented. Emissivities are estimated using equation 3 (no cloud-precipitation correction term is considered) and constrained in time by an emissivity atlas based on a Kalman filter algorithm (Krzeminski et al. 2009). Hereafter, these emissivity estimates are mentioned as clear-sky retrievals. In conclusion, comparing the retrievals obtained in the all-sky framework with independent emissivity clear-sky estimates, we can verify the computational implementation of the cloud-precipitation correction term. This study examines AMSU-A (NOAA-18) observations (from 1 to 31 October 2011) all-sky versus clear-sky emissivity retrievals in channel 3 (50.3 GHz) and channel 15 (89 GHz). In order to analyse different atmospheric scenes, no quality control is applied.

The agreement between the two emissivity retrievals was examined like in the previous section. Statistical measures of the computations have again been evaluated using RMS differences and Pearson coefficients. They are summarised in table 3. Scatter plots, histograms and mean emissivity maps (figures 5–8) show that emissivity estimates in the all-sky approach are comparable to those provided by the clear-sky computation, confirming that the cloud-precipitation correction term introduced in equation 5 brings reasonable emissivity estimations.

At 50.3 GHz, very slight differences are observed. Globally, RMS differences are very low (0.011) and correlation coefficients are greater than 91% in each geographical area. It is reasonable observing a negligible contribution from the cloud-precipitation term as the cloud contamination is not a dominant process at this frequency. However, mean emissivity maps of difference between all-sky and clear-sky retrievals (figure 7) show positive and a very small number of negative biases coming from the cloud-precipitation term implementation. At 89 GHz, on the contrary, the cloud-precipitation term introduced in the emissivity computation produces more differences. Globally, RMS is doubled (0.022) and correlation coefficient in the Northern hemisphere drops to 85%. Mean emissivity maps of difference between all-sky and clear-sky retrievals (figure 8) show slightly larger positive biases. Negative biases are still observed, however not as many as the positive. Global mean differences between all-sky and clear-sky emissivities (all-sky minus clear sky) computed over the whole sample of retrievals at 50.3 and 89 GHz

	R (%)				RMS			
Freq (GHz)	G	NH	T	SH	G	NH	T	SH
50.3	93	95	92	94	0.011	0.009	0.015	0.011
89	91	85	95	93	0.022	0.022	0.023	0.021

Table 3: Pearson correlation (R) coefficients and root mean square (RMS) differences for AMSU-A all-sky and clear-sky emissivity estimates. Calculations for AMSU-A channel 3 (50.3 GHz) and 15 (89 GHz) were conducted globally [60,-60], G, Northern hemisphere [60,20], NH, Tropics [20,-20], T, and Southern hemisphere [-20,-60], SH. The sample of observations is from 1 to 31 October 2011.

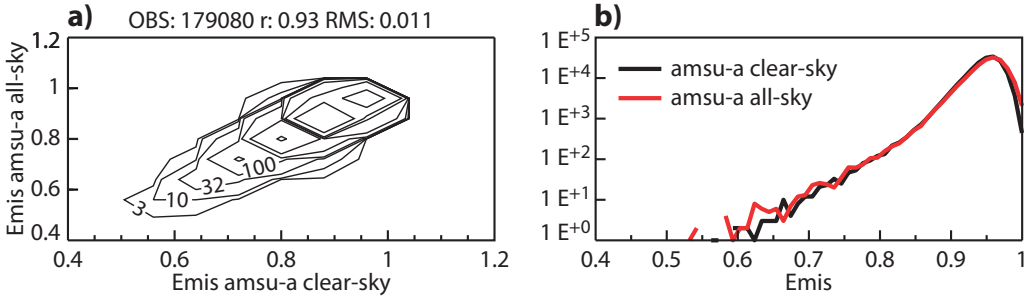

Figure 5: Scatter plot, a, and histogram, b, of AMSU-A channel 3 (50.3 GHz) all-sky versus clear-sky emissivity retrievals. The sample of observations is 1 month of data (1-31 October 2011) and latitude ranges from -60 to 60 degrees. The scatter plot density is represented by logarithmic contours at 3, 10, 32, 100 and so on, per 0.08 by 0.08 bin. Number of observations (OBS), Pearson correlation coefficients (r) and root mean square (RMS) differences are also shown. Histogram bin size is 0.01. Logarithmic scale is used on the y-axis.

show positive values of 0.0029 and 0.0024, respectively. In the Tropics, where the positive biases are mainly localised, the mean of emissivity differences is 0.0069 at channel 3 and 0.0086 at channel 15. These results suggest that the introduction of the cloud-precipitation term slightly increases the emissivity estimation. Scattering processes due to clouds and precipitation in radiative transfer calculations cool the resultant simulated radiances. The atmospheric down-welling and up-welling radiation and the atmospheric transmissivity of the RTTOV-SCATT cloudy column ($T^{\downarrow}_{cld}(\theta,\nu)$, $T^{\uparrow}_{cld}(\theta,\nu)$ and Γ_{cld}) are the parameters directly involved in the cloudy emissivity estimation (equation 5). As a consequence, the slight and positive increase of the emissivity estimation might be considered as the response to the cooling of the simulated brightness temperatures.

In order to understand if the location of the emissivity biases is reasonable with the all-sky retrieval implementation, we can consider the mean total hydrometeor content map as an indicator of cloudiness

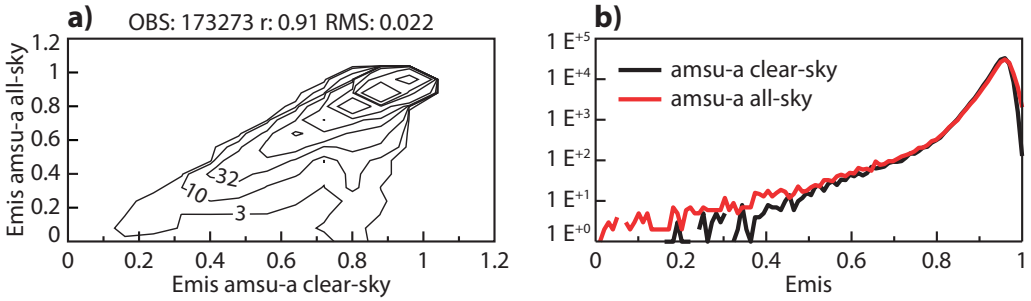

Figure 6: As figure 5, but for AMSU-A channel 15 (89 GHz).

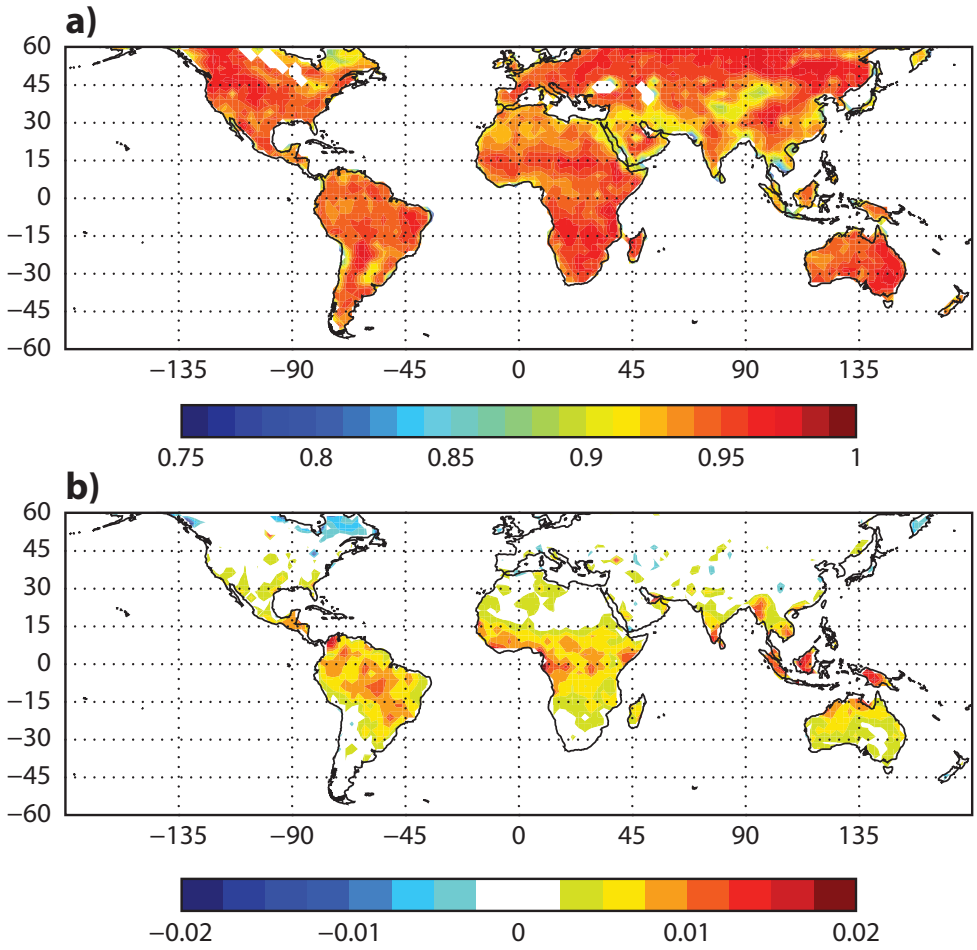

Figure 7: Mean land emissivity maps of AMSU-A channel 3 (50.3 GHz) retrievals: all-sky, a, and difference between all-sky and clear-sky (all-sky minus clear-sky), b. Maps are binned in 2.5 by 2.5 boxes over 1 month of data (1-31 October 2011).

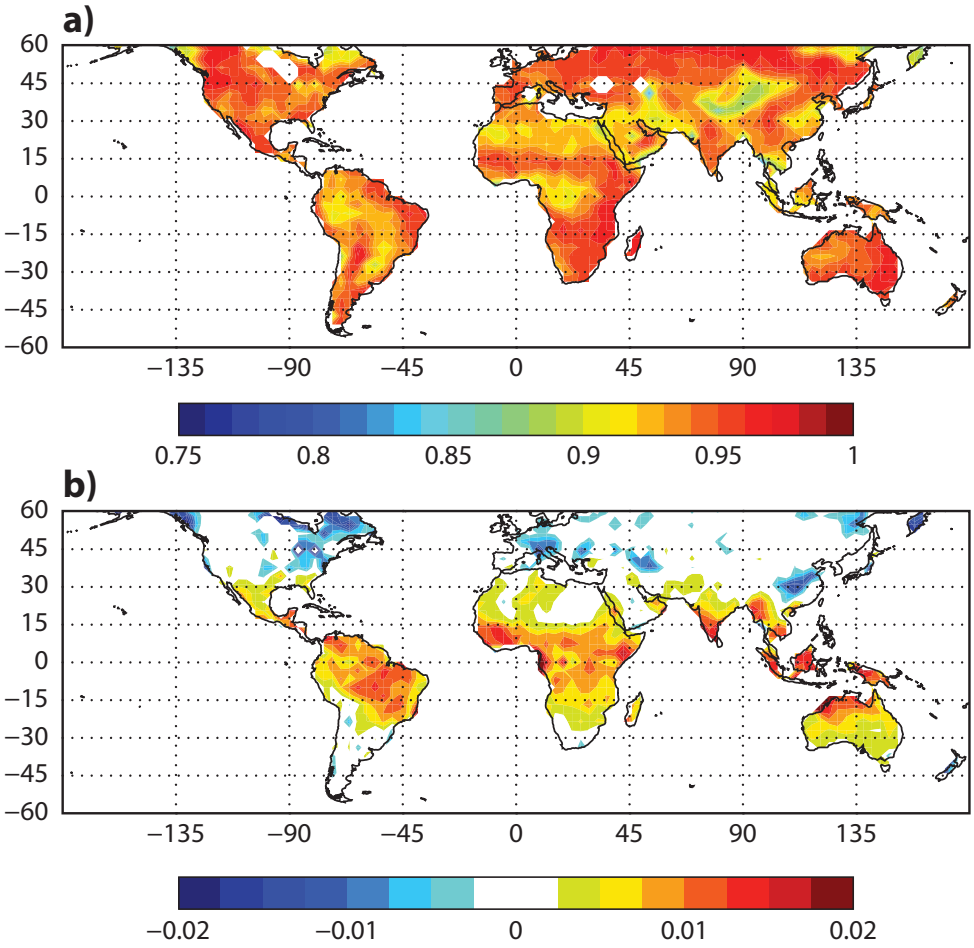

Figure 8: As figure 7, but for AMSU-A channel 15 (89 GHz).

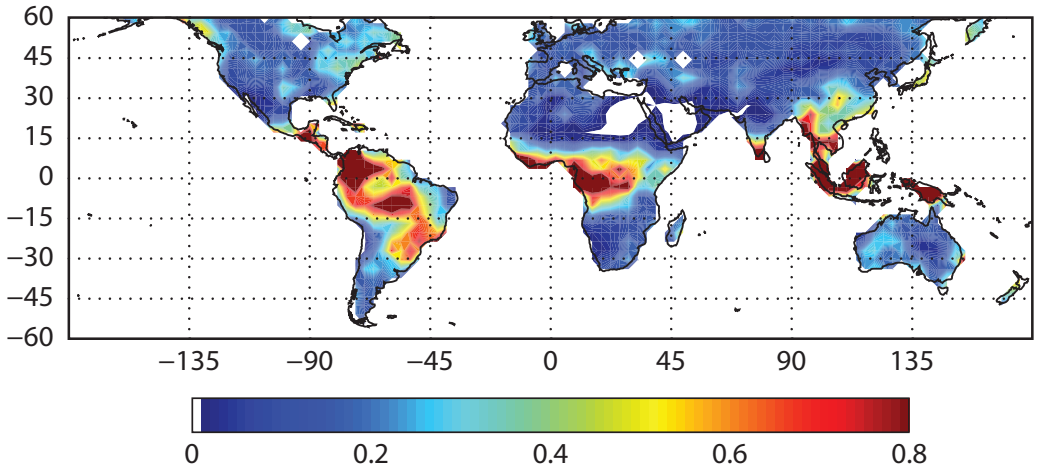

Figure 9: Mean total hydrometeor content map. The total hydrometeor content is given by the sum of model first guess cloud, rain, snow and ice water path (kg/m^2) Maps are binned in 2.5 by 2.5 boxes over 1 month of data (1-31 October 2011).

(figure 9). The biases observed at 50.3 and 89 GHz are related to regions with large hydrometeor amount and therefore consistent with the all-sky implementation. It is also worth pointing out that, at 89 GHz, in both the all-sky and clear-sky retrievals, a few retrievals show low emissivity estimates which might be unlikely. This is the same result we described in the previous sections for SSMI/S retrievals at 91h and 91v. The result confirms that, at higher microwave frequencies, independently of the sensor, observation geometry and the scheme implemented (clear-sky or all-sky), the emissivity retrieval is more affected by cloud contamination and consequently it might lead to retrievals which must be rejected.

3 Towards the assimilation of SSMI/S humidity sounding channels over land

3.1 Introduction

Differences between observations and simulated brightness temperatures, so-called first guess departures, must be investigated to understand which set of data might be selected for the assimilation. An unbiased, symmetric and Gaussian distribution of first guess departure is one necessary 4D-Var assumption that must be satisfied before any sample of observations can be considered for an assimilation experiment. This section attempts to work out the causes that lead to non-Gaussian distributions and to identify the best screening strategy to reject those observations affected by large departures.

In this study, land emissivity retrieved from SSMI/S channel 18 (91 GHz, horizontal polarization), was given to the humidity sounding channels (channel 9, 10 and 11). Subsequently, SSMI/S first guess departures were computed by running assimilation experiments, using the incremental 4D-Var ECMWF system at T255 horizontal resolution ($\sim$78 km), from August to October 2011. SSMI/S F17 observations over land were only passively introduced into the system. The initial SSMI/S data set collects observations over 1 month (1-31 August 2011) and for latitudes ranging from -60 to 60 degrees, giving a total of 330543 observations over land. From this initial sample of observations, the retrieval at 91h produces 314276 emissivity estimates (95% of observations), while only 5% of retrievals must be rejected (unacceptable values, for instance greater than 1). As a result, every initial sample of SSMI/S humidity

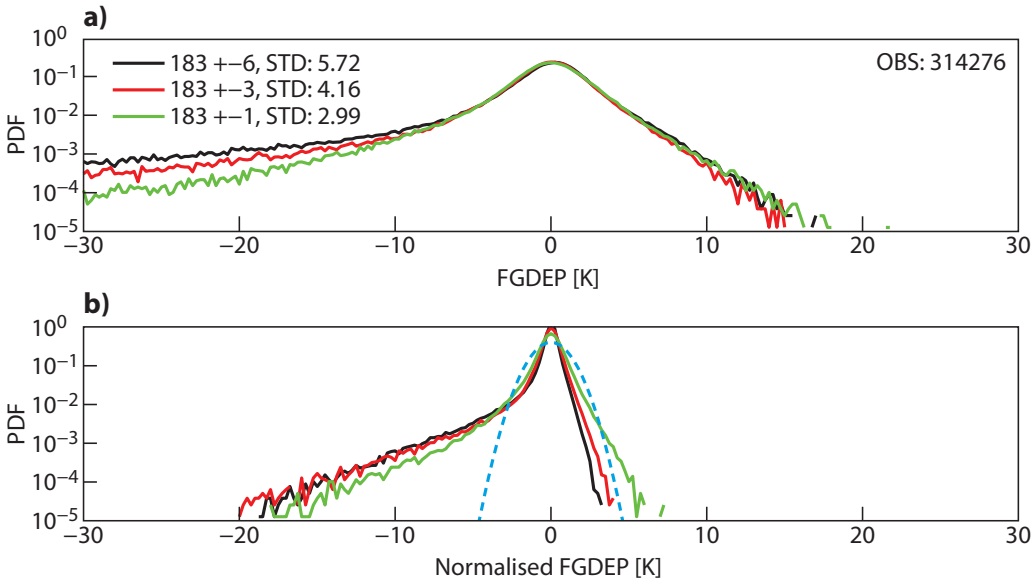

Figure 10: PDFs of SSMI/S humidity sounding channel first guess departures: a, distribution corresponding to those observations where land surface emissivity has been retrieved from channel 18 (91h), b, as in a, but normalised by the standard deviation (STD) of the whole sample. Black line is for channel 9 (183.31 ± 6.6), red line for channel 10 (183.31 ± 3.0) and green line for channel 11 (183.31 ± 1.0). In panel a, number of observations (OBS) and standard deviations of each sample are also provided. In panel b, the dotted blue line gives the Gaussian distribution as a reference. The sample of observations is 1 month of data (1-31 August 2011) and latitude ranges from -60 to 60 degrees.

sounding data is characterised by 314276 observations.

Figure 10 encapsulates the nature of the initial problem: the distribution of SSMI/S humidity sounding channel first guess departures is far from symmetric and Gaussian. The initial sample of observations cannot be considered for an assimilation experiment. Large positive and negative first guess departures are observed, with negative values greater than -40 K. Standard deviations computed over the whole first guess departure sample are also quite large: 5.72 K for channel 9, 4.16 K for channel 10 and 2.99 K for channel 11. Standard deviations seem to decrease with increasing channel number. Channel at 183.31 ± 6.6 GHz is more affected by surface conditions than the other two channels which might explain the largest standard deviations. However, our land surface emissivity estimates, even though affected by errors and retrieved using a different frequency, cannot be the cause of such large inconsistencies.

The source of the problem is shown in scatter plots and histograms of SSMI/S humidity sounding observations and simulated radiances (figure 11 and 12, respectively). Globally, the computation of first guess brightness temperatures is not accurate enough leading to significant differences with observed radiances. Simulated radiances do not go lower than 220 K, whilst observations are colder, reaching values of 180 K. Channel 11 (183.31 ± 1.0 GHz) seems to be the channel least affected by this result, but this might be again explained by the different channels sensitivity. Channel 11 is characterised by a weighting function that peaks at about 6 km. Radiative transfer calculations for this channel might be less affected by surface conditions and cloud contamination leading to better simulated radiances. The deficiencies in radiative transfer calculations can be localised in the Northern hemisphere and in the Tropics, where scatter plots are similar to those presented in figure 11. In such regions, observations and first guess brightness temperatures have also lower correlation and higher RMS differences than the Southern hemisphere (Pearson correlation coefficients and RMS differences are summarised in table 4).

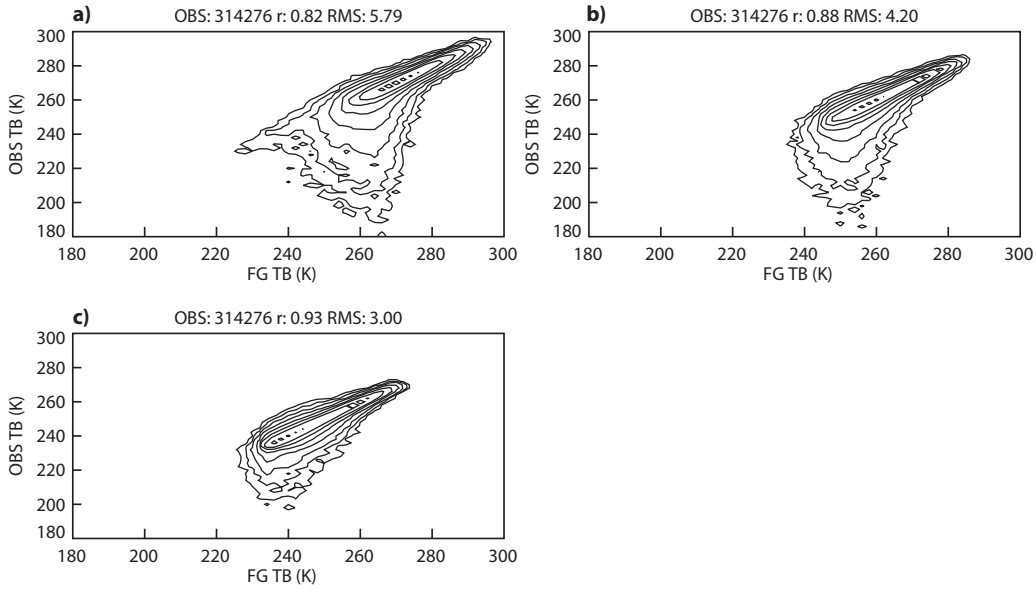

Figure 11: Scatter plots of SSMI/S humidity sounding observations (OBS TB) versus first guess brightness temperatures (FG TB): a, channel 9 (183.31 $\pm$ 6.6 GHz), b, channel 10 (183.31 $\pm$ 3.0 GHz), c, channel 11 (183.31 $\pm$ 1.0 GHz). The sample of observations is 1 month of data (1-31 August 2011), where land surface emissivities were retrieved from channel 18 (91h). Latitude ranges from -60 to 60 degrees. The scatter plot density is represented by logarithmic contours at 3, 10, 32, 100 and so on, per 2 by 2 K bin. Number of observations (OBS), Pearson correlation coefficients (r) and root mean square (RMS) differences are also shown.

As a consequence, in the Northern hemisphere and in the Tropics, PDFs of SSMI/S humidity sounding observations and first guess brightness temperatures show significant disagreement, whilst in the Southern hemisphere, where the observed radiances are not affected by large depressions, the resultant distributions are similar. This result is summarised in figure 12 for 183.31 $\pm$ 6.6 GHz only, because the other two humidity channels have same behaviour.

The limitation of the all-sky assimilation over land for these high microwave frequencies is intrinsic to RTTOV-SCATT calculations. As already described in section 2.2, the observation operator in the all-sky approach is RTTOV-SCATT, which provides scattering radiative transfer calculations at microwave frequencies. Scattering properties are pre-calculated using Mie theory and tabulated as function of frequencies, temperature and hydrometer type and density. Over a radiative warm surface like land, scat-

Initial sample of SSMI/S observations over land: 314276								
	R (%)				RMS (K)			
Freq (GHz)	G	NH	T	SH	G	NH	T	SH
183.31 $\pm$ 6.6	82	83	76	93	5.70	5.39	7.30	3.47
183.31 $\pm$ 3.0	88	89	85	95	4.20	3.80	5.42	2.61
183.31 $\pm$ 1.0	93	93	91	96	3.00	2.78	3.72	2.16

Table 4: Pearson correlation (R) coefficients and root mean square (RMS) differences for SSMI/S observations and first guess brightness temperatures. Calculations for SSMI/S humidity sounding channels were conducted globally [60,-60], G, Northern hemisphere [60,20], NH, Tropics [20,-20], T, and Southern hemisphere [-20,-60], SH. The sample of observations is 1 month of data (1-31 August 2011), where land surface emissivities were retrieved from channel 18 (91h).

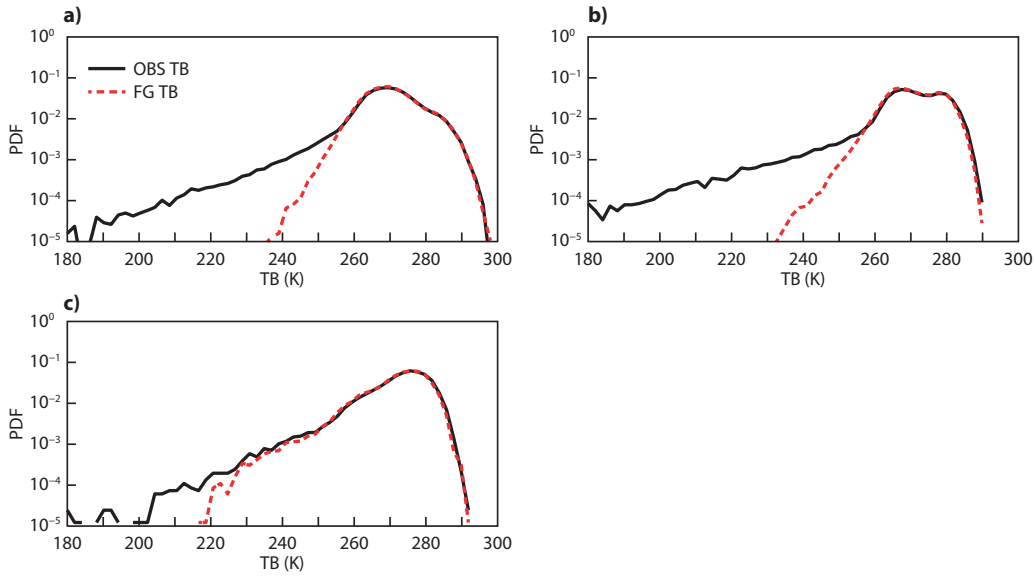

Figure 12: PDFs of SSMI/S channel 9 (183.31 $\pm$ 6.6 GHz) observations (OBS TB), black line, and first guess brightness temperatures (FG TB), red dotted line: a, Northern hemisphere [20,60], b, Tropics [-20,20], c, Southern hemisphere [-20,-60]. The sample of observations is 1 month of data (1-31 August 2011), where land surface emissivities were retrieved from channel 18 (91h). Histogram bin size is 2 K. Logarithmic scale is used on the y-axis.

tering from solid hydrometeors causes strong brightness temperature depressions in higher microwave frequencies (above 85 GHz). Figure 13 shows the map of the mean total hydrometeor content (given by the sum of model first guess cloud, rain, snow and ice water path) that can be considered as a good indicator of cloudiness. Between -15 and 30 degree latitude, the mean total hydrometeor content has the largest values and it likely identifies areas mainly affected by ice scattering particles. This might explain the better simulation of first guess radiances in the Southern hemisphere (-20,-60). The Mie soft sphere approximation used to represent snow and ice in our radiative transfer calculations seems to be not accurate enough. Shapes and densities of ice and snow particles have a significant rule in the computation of simulated radiances. For instance, Evans and Stephens (1995 and 1995a) simulated the scattering properties of ice particles and found that the particle shape has significant effects: a range of about three is found in extinction over five different shapes (solid and hollow columns, hexagonal plates, planar bullet rosettes, and equivalent-volume spheres) for the same size distribution and ice water content. The characteristic particle size has the greatest impact on the extinction and single scattering albedo while the particle size distribution plays a minor role. Doherty et al. (2007) also found that the density of the ice particles significantly affects the interpretation of the sensor radiances using radiative transfer models. Work at ECMWF is currently ongoing to improve RTTOV-SCATT simulations and investigate the possibility to migrate from Mie sphere approximation to more appropriate shapes. For the moment, a screening method to eliminate all those profiles which cause large inconsistency between observations and simulated radiances must be investigated. The next sections describe the strategy adopted.

3.2 Scattering index

Typical atmospheric hydrometeors have sizes around 0.01 mm for liquid cloud drops and 0.1 to 1 mm for drizzle and rain drops. Ice crystals are similar in size to rain drops, although exceptionally snowflakes and ice aggregates associated with large cumulus can reach sizes of 10 mm. When the wavelength of

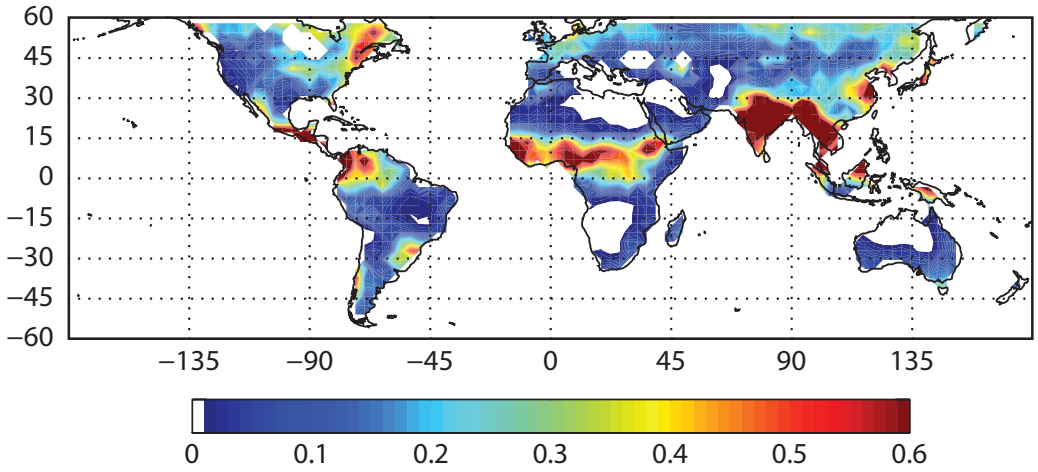

Figure 13: Mean total hydrometeor content map. The total hydrometeor content is given by the sum of model first guess cloud, rain, snow and ice water path (kg/m^2) Maps are binned in 2.5 by 2.5 boxes over 1 month of data (1-31 August 2011).

an observation is long compared to the hydrometeor size, scattering can be considered negligible. For most rain and ice hydrometeors scattering processes become important at wavelengths below around 5 mm (frequency $>$ 60 GHz). Over a warm radiative surface such as land, hydrometeor scattering can be very obvious and the observed radiances at high microwave frequencies (85 to 190 GHz) can be affected by large depressions. However, some land surfaces characterised by low emissivity, such as snow, ice and desert, can give a false scattering signature in clear-sky observations. Difficulties can also be caused by melting snow particles or low density snow flakes. These ice particles, when they melt, create paths of liquid water through the crystal which will absorb radiation strongly because of their length. In this situation, the absorption becomes very strong and the brightness temperatures are raised.

The SSM/I rainfall rate algorithm developed by Ferraro and Marks (1995) makes use of the scattering of up-welling radiation by precipitating cloud ice particles and large raindrops at 85.5 GHz to detect rainfall both over land and oceans. The difference between observed and clear-sky (through 19.35 GHz and 22.235 GHz vertical polarization observations) brightness temperatures at 85.5 GHz vertical polarization, which is referred to as the scattering index (SI) in Grody (1991), is calculated as follows:

$$SI = a + bT_{obs}^{19v} + cT_{obs}^{22v} + d(T_{obs}^{22v})^2 - T_{obs}^{85v}, \tag{6}$$

where, a, b, c and d are coefficients derived from SSM/I observations to estimate radiances observed at 85.5 GHz vertical polarization. More recently, Sun and Weng (2008) developed a set of empirical linear remapping coefficients to apply to F16 SSM/I-like channels. The authors conclude that SSMI/S F16 data can be successfully used in the retrievals previously developed for SSM/I channels. In particular, the SSM/I-like scattering index is as in equation 6, but the observed radiances change from 85.5 to 91.655 GHz and the coefficients a, b, c and d are defined as follows: 438.5, -0.46, -1.735 and 0.00589.

The use of the SI developed by Sun and Weng was investigated as potential parameter to localise and isolate scattering areas. However, the authors suggest that the SSMI/S to SSM/I remapping requires further improvement over the simple linear remapping algorithm used to correct the change from 85.5 to 91.655 GHz which cannot account for scattering and emission effects under all weather and surface conditions. As a consequence, the choice of the SSM/I-like SI might be not optimal in our context

considering that we make use of SSMI/S F17 observations in all-sky conditions over land. For this reason, two different types of scattering index have been also investigated.

Bennartz and Bauer (2003) studied the response of passive microwave observations to ice particle scattering and surface emissivity for frequencies at 85, 150 and 183 GHz. They found that a channel around 150 GHz exhibits the strongest scattering signature due to precipitation-sized ice particles and is only moderately affected by variations in surface emissivity. On the contrary, channels at around 85 GHz are much more strongly affected by variable surface emissivity and show smaller scattering signature. Bennartz et al. (2002) described a set of algorithms for nowcasting applications to identify precipitation and classify it according to its intensity. They found that, over both ocean and land, MHS channel at 150 GHz allows for better discrimination of different types of precipitation than the 89 GHz channels. More recently, Sun and Weng (2012) developed a retrieval algorithm to estimate the ice particle effective diameter and ice water path from SSMI/S observations. The measurements at 91.655 and 150 GHz are used as primary channels in the applications considering their high sensitivity to scattering and ice particles.

Considering the investigations carried out in literature, the choice of different types of scattering index was oriented towards the use of SSMI/S observations at 91.655 and 150 GHz. The first SI was defined as frequencies difference at channel 18 and channel 8 (91h - 150h), and the second as frequencies and polarizations difference at channel 17 and channel 8 (91v - 150h). To summarise, in order to localise scattering areas, we used SSMI/S brightness temperatures at different channels to define three distinct SI as follows:

a. SI[SSM/I-like] = 438.5 - 0.46 T_{obs}^{19v} - 1.735 T_{obs}^{22v} + 0.00589 $(T_{obs}^{22v})^2$ - T_{obs}^{91v},

b. SI[91h-150h] = T_{obs}^{91h} - T_{obs}^{150h},

c. SI[91v-150h] = T_{obs}^{91v} - T_{obs}^{150h}.

To examine the behaviour of SSMI/S first guess departures humidity sounding channels, standard deviation, mean and number of first guess departures were binned as a function of the scattering index computed according to a, b and c. We obtained very interesting similarities: for increasing values of the scattering index (values greater than 0), standard deviation increases, whilst the mean assumes larger negative values. Hence, we can infer that the SI is helpful to localise those observations which cannot be properly simulated by RTTOV-SCATT, producing large negative first guess departures. First guess departures binned with respect to a, b and c are also characterised by a scattering index region where standard deviation and mean are approximately constant and respectively equal to 2 and 0. We can reasonably classify these areas as those regions where observations are not strongly affected by rain and ice hydrometeor scattering processes. As mentioned before, all three scattering indeces give similar results. As a consequence, we only present SSMI/S first guess departures humidity sounding channels binned as a function of the scattering index c (figure 14 and 15). As it can be easily done from figure 15, we graphically deduced regions with constant standard deviation and mean of first guess departures for every scattering index investigated:

a. 0 K $<$ SI[SSM/I-like] $<$ 6 K,

b. -15 K $<$ SI[91h-150h] $<$ 0 K,

c. -4 K $<$ SI[91v-150h] $<$ 4 K.

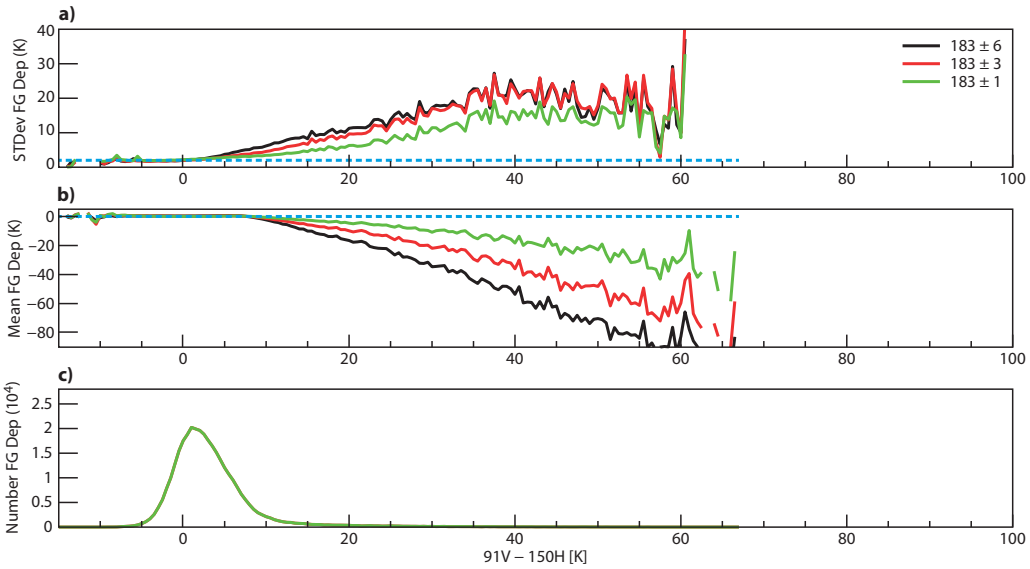

Figure 14: Standard deviation, a, mean, b, and number, c, of SSMI/S humidity sounding channel first guess departures, binned as a function of SI given by SSMI/S frequencies and polarizations difference (91v - 150h): channel 9 (183.31 $\pm$ 6.6), black line, channel 10 (183.31 $\pm$ 3.0), red line, and channel 11 (183.31 $\pm$ 1.0), green line. Bin size is 0.5 K. Blue dotted line in a indicates constant standard deviation equals 2, whilst in b constant mean equals 0. The sample of observations is 1 month of data (1-31 August 2011), where land surface emissivities were retrieved from channel 18 (91h).

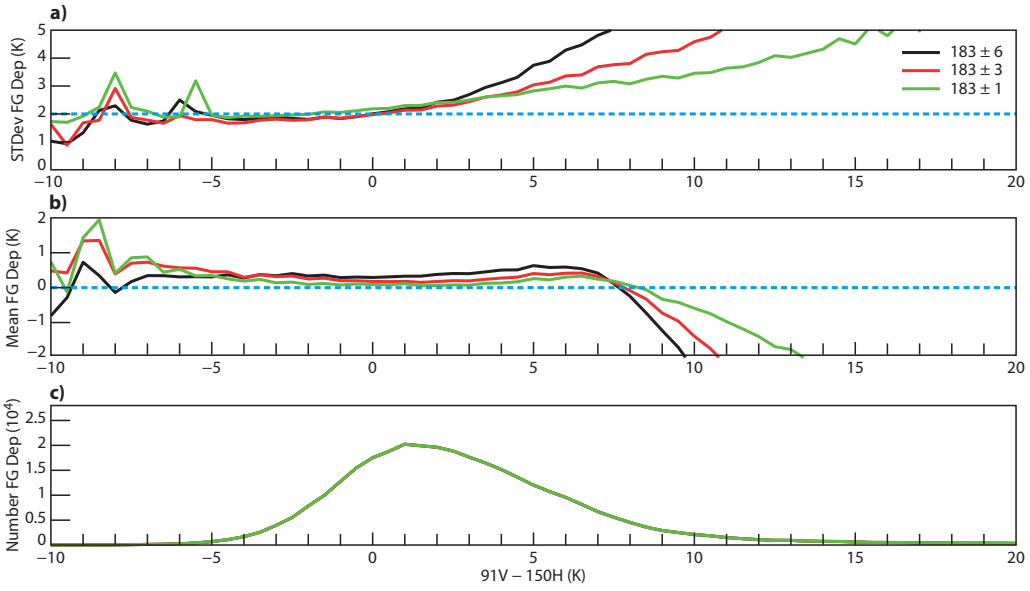

Figure 15: As figure 14, but zoomed in.

Thresholds a, b and c were also chosen to not take into account the spikes in standard deviation and mean of first guess departures that are visible on the left side of the SI domain considered. They are probably due to sampling issues and, considering the very few observations in those bins, they can be assumed insignificant. It is worth mentioning that our scattering index derivation is based on observations only. The use of a symmetric SI, that could take also into account simulated radiances (for instance $[SI_{obs} + SI_{fg}]/2$), would be more appropriate to investigate mean first guess departures biases. However, radiative transfer calculations at 91.655 and 150 GHz are not enough accurate to consider a symmetric approach. We will discuss it again in the next section.

Aside from these difficulties, thresholds a, b and c might be considered capable at detecting regions where scattering processes are not dominant. In fact, the NESDIS SSMI/S algorithm that implements the SSM/I-like scattering index uses SI values greater than 10 K to identify scattering situations. Thresholds b and c, on the other hand, are in agreement with the strong scattering signature that characterises channels around 150 GHz. Independently of polarization type, in areas affected by strong rain and ice hydrometeors scattering processes, brightness temperatures at 150 GHz are colder than radiances at 91.655. Hence, increasing the scattering processes, the positive difference between 91.655 and 150 GHz increases.

In order to choose the best SI for data screening, we analysed the latitude and longitude locations of SSMI/S observations in respect to the total hydrometeor content. The total hydrometeor content represents a good indicator of cloudiness and therefore it can be used as a reference to understand if thresholds a, b and c are reasonable predictors to estimate areas less affected by scattering processes. Figure 16 shows that screenings b and c are able to detect regions with low hydrometeor content, whilst the SSM/I-like scattering index seems unable to reject observations over Central Africa and India, where hydrometeor amount predicted by the model is large. This inconsistency can be explained by the fact that coefficients a, b c and d of equation 6 are not optimal for F-17 observations.

Considering the findings of this study, the use of the SI defined as SSMI/S observation difference between channel 17 and channel 8 (91v - 150h) was taken as the best screening methodology. Starting from an initial sample of 314276 observations, the use of the SI[91v-150h] screening detects 213227 observations which, according to latitude and longitude location, are correlated with regions of low hydrometeor content predicted by the model. It means that, most likely, intense scattering areas are avoided, but, possibly, these areas are still affected by cloudy-precipitation observations. Finally, polarization difference between the two channels might also help to reject observations over high orography. This is suggested by figure 16 (panel c) where a low number of observations seem to be selected over high orography areas such as Andes and Himalaya.

In addition, to give a statistical measure to the sample of observations selected within and outside the threshold c, we computed Pearson correlation coefficients and root mean square differences for SSMI/S radiances and the corresponding modelled brightness temperatures. Calculations were conducted globally (60,-60), for the Northern hemisphere (60,20), Tropics (20,-20), and Southern hemisphere (-20,-60). The findings show that, when the scattering index screening is applied, independently of the channel and geographical area, observed and modelled radiances have the highest correlation and the lowest RMS differences (summary in table 5). This result is also encapsulated in figure 17 which shows, as a reference, scatter plots of observed and first guess radiances for channel 9 (183.31 ± 6.6 GHz), within and outside the scattering index domain. As a conclusion, a SI screening strategy seems to be necessary to reduce deficiencies in radiative transfer calculations and move towards a possible assimilation of SSMI/S humidity sounding channels over land.

As a final test, figure 18 shows first guess departures in the SSMI/S humidity sounding channels cor-

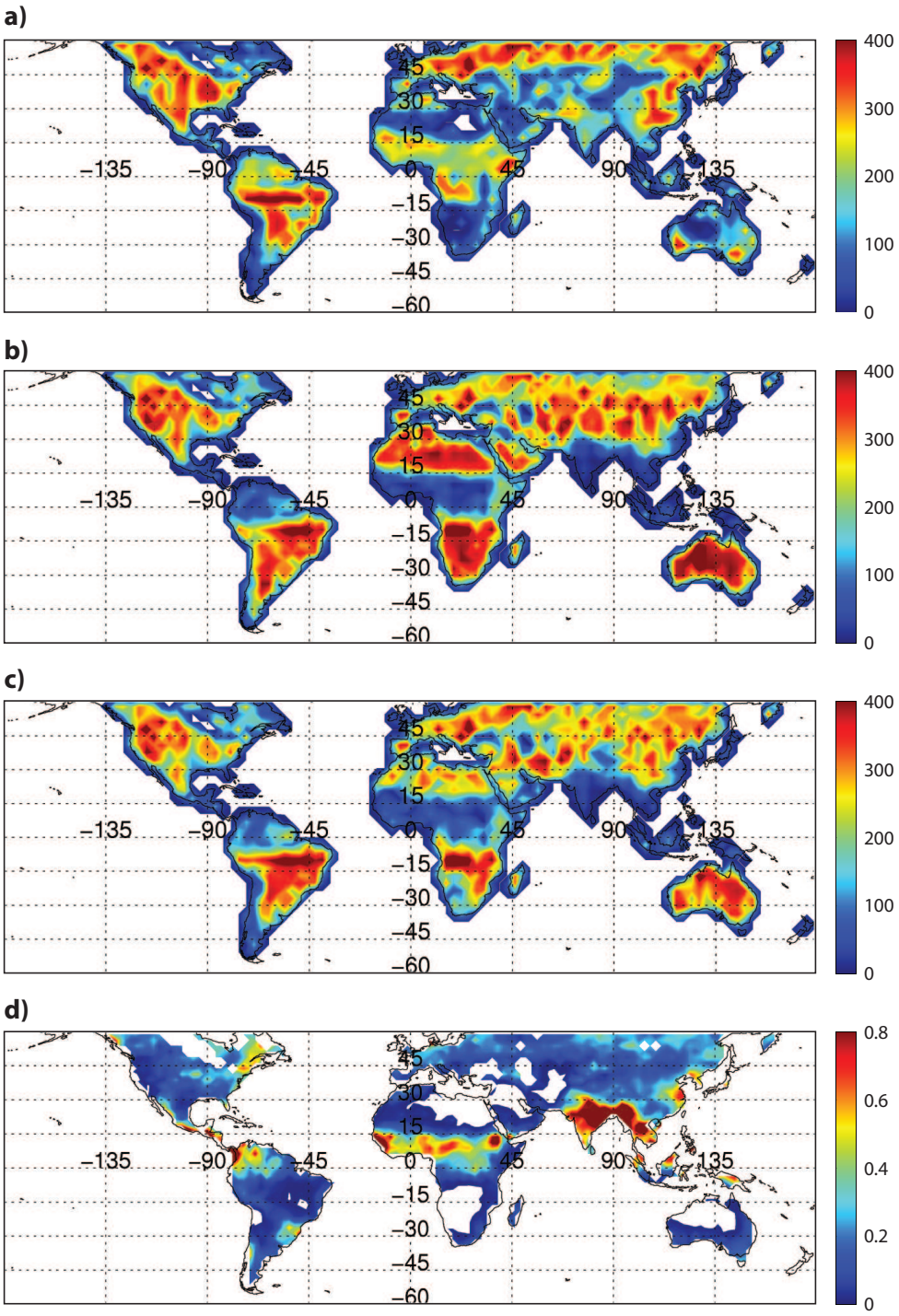

Figure 16: Mean number maps of SSMI/S observations according to scattering index thresholds: a, 0 K < SI[SSM/I-like] < 6 K, b, -15 K < SI[91h-150h] < 0 K, c, -4 K < SI[91v-150h] < 4 K. In panel d, mean total hydrometeor content map, as an indicator of cloudiness. The total hydrometeor content is given by the sum of model first guess cloud, rain, snow and ice water path (kg/m^2). Maps are binned in 2.5 by 2.5 boxes over 1 month of data (1-31 August 2011), where land surface emissivities were retrieved from channel 18 (91h).

Initial sample of SSMI/S observations over land: 314276								
SI = 91v−150h	-4 K < SI < 4 K							
	R (%)				RMS (K)			
Freq (GHz)	G	NH	T	SH	G	NH	T	SH
183.31 ± 6.6	95	94	94	96	2.05	2.18	1.88	1.66
183.31 ± 3.0	96	95	96	97	2.01	2.11	1.89	1.72
183.31 ± 1.0	96	95	96	97	2.22	2.27	2.22	1.92
	SI < -4 K and SI > 4 K							
	R (%)				RMS (K)			
Freq (GHz)	G	NH	T	SH	G	NH	T	SH
183.31 ± 6.6	69	73	54	89	9.77	9.48	11.03	6.01
183.31 ± 3.0	76	79	60	92	6.80	6.30	8.06	4.09
183.31 ± 1.0	86	88	72	95	4.21	3.77	5.10	2.68

Table 5: Pearson correlation (R) coefficients and root mean square (RMS) differences for SSMI/S observations and modelled radiances according to scattering index given by SSMI/S frequency and polarization difference (91v - 150h). Calculations for SSMI/S humidity sounding channels were conducted globally [60,-60], G, Northern hemisphere [60,20], NH, Tropics [20,-20], T and Southern hemisphere [-20,-60], SH. The sample of observations is 1 month of data (1-31 August 2011), where land surface emissivities were retrieved from channel 18 (91h).

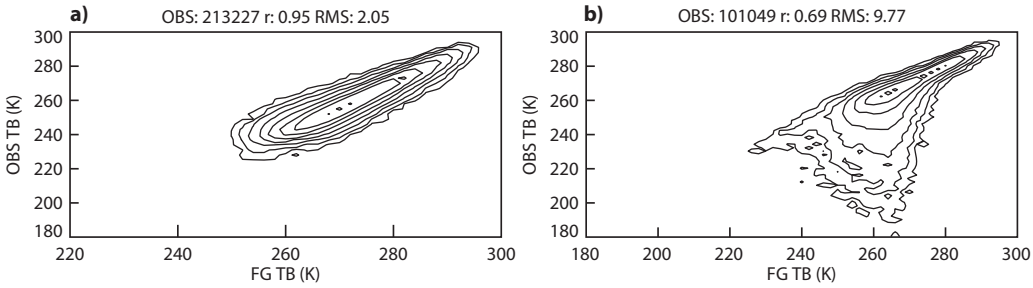

Figure 17: Scatter plots of SSMI/S channel 9 (183.31 ± 6.6 GHz) observations (OBS TB) versus first guess brightness temperatures (FG TB): a, observations where -4 K < SI[91v-150h] < 4 K; b, observations where SI[91v-150h] < -4 K and SI[91v-150h] > 4 K. The sample of observations is 1 month of data (1-31 August 2011), where land surface emissivities were retrieved from channel 18 (91h). Latitude ranges from -60 to 60 degrees. The scatter plot density is represented by logarithmic contours at 3, 10, 32, 100 and so on, per 2 by 2 K bin. Number of observations (OBS), Pearson correlation coefficients (r) and root mean square (RMS) differences are also shown.

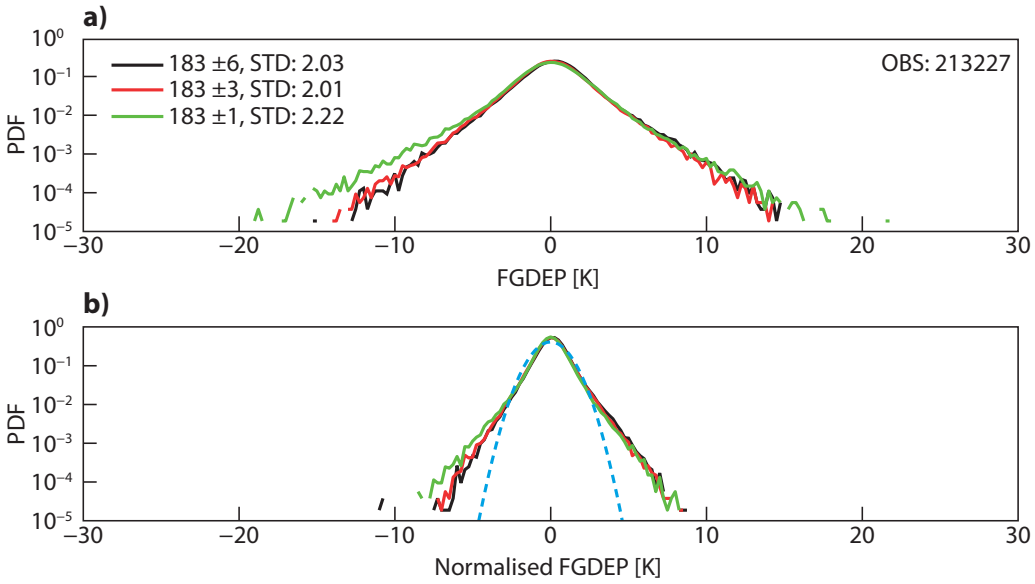

Figure 18: PDFs of SSMI/S humidity sounding channel first guess departures: a, distribution corresponding to those observations where -4 K $<$ SI[91v-150h] $<$ 4 K, b, as in a, but normalised by the standard deviation (STD) of the whole sample. Black line is for channel 9 (183.31 $\pm$ 6.6), red line for channel 10 (183.31 $\pm$ 3.0) and green line for channel 11 (183.31 $\pm$ 1.0). In panel a, number of observations (OBS) and standard deviations of each sample are also provided. In panel b, the dotted blue line gives the Gaussian distribution as a reference. The sample of observations is 1 month of data (1-31 August 2011), where land surface emissivities were retrieved from channel 18 (91h). Latitude ranges from -60 to 60 degrees.

responding to those observations selected within -4 K $<$ SI[91v-150h] $<$ 4 K. Comparing figure 18 to figure 10, we can quantify the improvements with respect to the initial sample of observations. We have now a distribution of first guess departure less biased and more symmetric and with smaller standard deviations: for channel 9 is now reduced to 2.03 K (5.72 K before), 2.01 K (4.16 K) for channel 10 and 2.22 K (2.99 K) for channel 11.

3.3 Verification against actively assimilated MHS observations

The SI screening is an effective strategy to reject those observations affected by intense rain and ice hydrometeor scattering processes. The resultant distribution of first guess departures (figure 18) is closer to a Gaussian shape than the initial sample of observations (figure 10). Scattering from snow and ice particles is not the only source of difficulty to take into account in the attempt of assimilating observations over land. Variability of hydrometeor distribution, cloud and precipitation and surface conditions needs to be considered as well. Essentially, these features might be badly located, poorly shaped or have incorrect intensity in the first guess compared to the observations. This is often referred to as mislocation error. Geer et al. (2011) investigated first guess departures of microwave imager window channel observations assimilated in all-sky conditions over ocean. First guess departure standard deviations were studied introducing a symmetric predictor based on cloud amount derived by both observations and simulations. By means of the symmetric cloud amount, the authors derived a robust error model that can be used to determine the size of observation errors and assimilate all-sky observations under the assumption of Gaussianity on which assimilation systems are based. In our study, due to RTTOV-SCATT deficiencies, we make use of an asymetric predictor (scattering index) based on observations only. Even though the observed SI is not a symmetric predictor (for instance given by $[SI_{obs} + SI_{fg}]/2$), the quality control

check is able to produce a reasonable unbiased and Gaussian distribution of first guess departures (figure 18). This might again be explained by deficiencies in radiative transfer calculations. The SI screening is good enough to correct the left wing of the distribution of the first guess departures distribution (large negative first guess departures biases of figure 10), whilst the right wing is basically not affected. The results might be different if radiative transfer calculations were more accurate. In the future, we will revisit this work using more appropriate ice single scattering properties to simulated observed brightness temperatures. For the moment, we can consider the observed SI screening as the best quality control check.

In panel b of figure 18, we can observe that the left and right wings of the distribution of SSMI/S humidity sounding channel first guess departures are slightly distant from the Gaussian distribution plotted as a reference. In order to remove these wings, we introduced other two additional screenings. Observations will be kept if:

a. -5 K $< T_{obs}^{ch}$ - $T_{clr}^{ch} <$ +5 K,

b. SWP and IWP $<$ 0.1 kg/m^2.

The screening a is based on the difference between the observed brightness temperature (T_{obs}) and the clear-sky part of the simulated radiance ignoring the effect of the hydrometeors (T_{clr}) at each SSMI/S humidity sounding channel (ch = channel 8, 9 and 10). This quality control is generally applied to window channels to reject cloud-affected observations. For instance, at ECMWF, MHS and AMSU-A observations over land are respectively rejected when: absolute value of channel 2 (150 GHz) first guess departures is greater than 5 K and absolute value of channel 4 (52.8 GHz) is greater than 0.7 K. In our context, we are dealing with humidity sounding channels so that screening a might help to resolve some residual RTTOV-SCATT deficiencies not detected by the SI check (negative first guess departure biases), but it might take into account cloudy observations as well. On the contrary, screening b, based on model snow and ice water path (SWP and IWP), is focused on detecting possible model mislocation errors, in other words, those observations which might be clear and the corresponding first guess cloudy, producing positive first guess departures.

Applying the additional quality control checks a and b, the resultant PDFs of SSMI/S humidity sounding channel first guess departures normalised by the standard deviation of the whole sample have very close Gaussian shape. This result is shown in figure 19. Figure 20 examines the resultant sample of humidity sounding observations, comparing observed radiances to the equivalent observations in model space by means of scatter plots. For every humidity sounding channel, the correlation is larger than 95% and the RMS differences lower than 1.70 K. This is a remarkable improvement considering the nature of the initial problem (figure 10 and table 4).

From the initial set of SSMI/S data over land, 330543 observations (1-31 August 2011), we achieved the following results:

1. the retrieval at 91h gives 95% of land surface emissivity estimates with emissivity values between 0 and 1 and 314276 observations were selected for the quality control checks;
2. the scattering index screening (91v-150h) is able to selected 213227 observations presumably not affected by intense rain and ice hydrometeor scattering processes;
3. the additional 2 quality control checks complete the process: 201011 observations, for channel 9, 200245 for channel 10 and 197850 for channel 11.

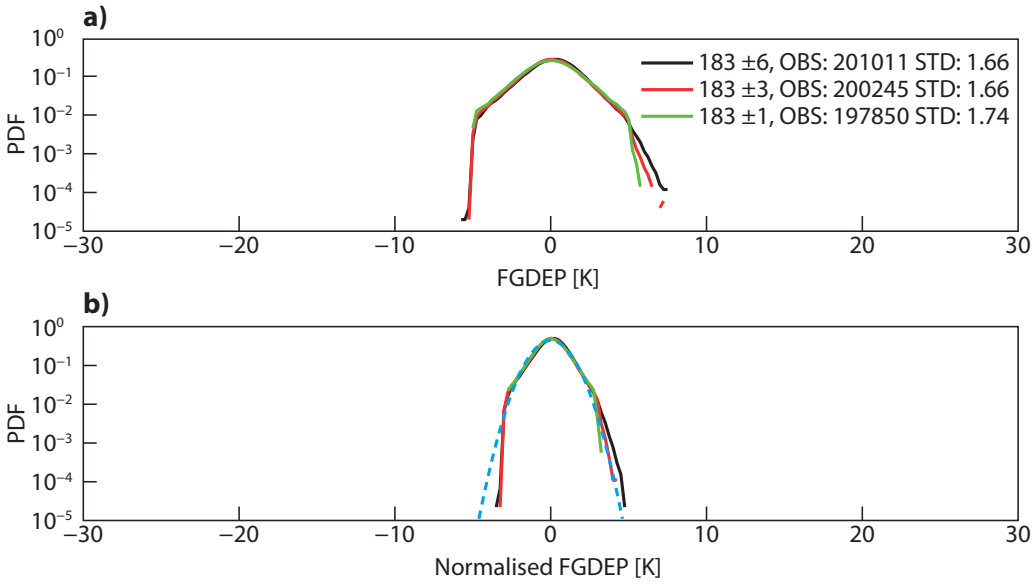

Figure 19: PDFs of SSMI/S humidity sounding channel first guess departures: a, distribution corresponding to those observations selected by the screening methodology, b, as in a, but normalised by the standard deviation (STD) of the whole sample. Black line is for channel 9 (183.31 ± 6.6), red line for channel 10 (183.31 ± 3.0) and green line for channel 11 (183.31 ± 1.0). In panel a, number of observations (OBS) and standard deviations of each sample are also provided. In panel b, the dotted blue line gives the Gaussian distribution as a reference. The sample of observations is 1 month of data (1-31 August 2011), where land surface emissivities were retrieved from channel 18 (91h). Latitude ranges from -60 to 60 degrees.

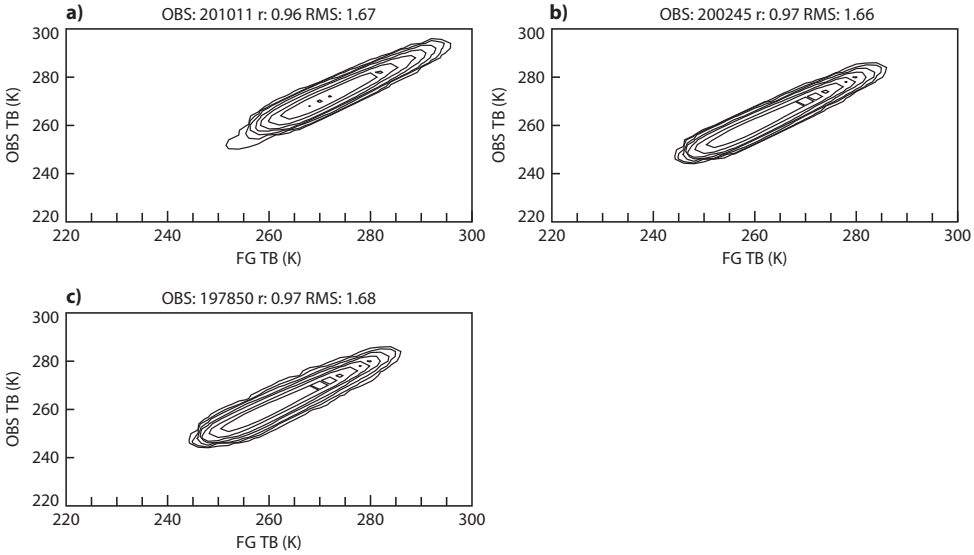

Figure 20: Scatter plots of SSMI/S humidity sounding observations (OBS TB) versus first guess brightness temperatures (FG TB) for those observations selected by the screening methodology: a, channel 9 (183.31 ± 6.6 GHz), b, channel 10 (183.31 ± 3.0 GHz), c, channel 11 (183.31 ± 1.0 GHz). The sample of observations is 1 month of data (1-31 August 2011), where land surface emissivities were retrieved from channel 18 (91h). Latitude ranges from -60 to 60 degrees. The scatter plot density is represented by logarithmic contours at 3, 10, 32, 100 and so on, per 2 by 2 K bin. Number of observations (OBS), Pearson correlation coefficients (r) and root mean square (RMS) differences are also shown.

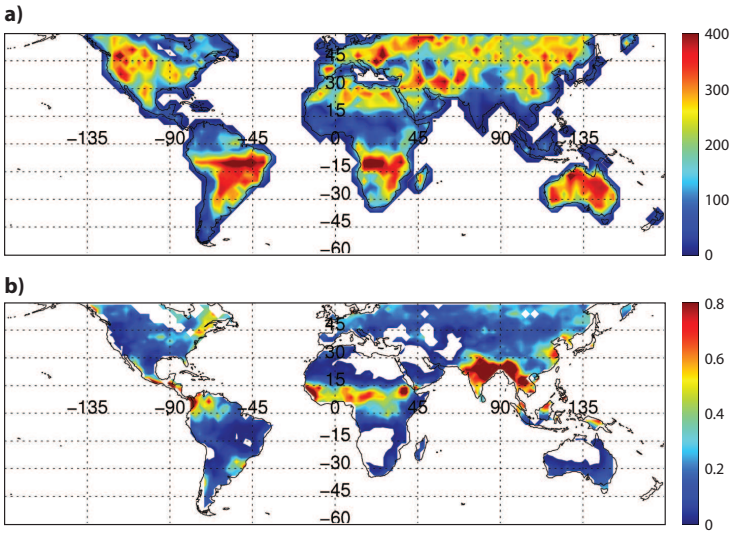

Figure 21: Mean number maps of SSMI/S channel 9 (183.31 $\pm$ 6.6) observations selected by the screening methodology (a). In panel b, mean total hydrometeor content map, as an indicator of cloudiness. The total hydrometeor content is given by the sum of model first guess cloud, rain, snow and ice water path (kg/m^2). Maps are binned in 2.5 by 2.5 boxes over 1 month of data (1-31 August 2011), where land surface emissivities were retrieved from channel 18 (91h).

The main result is the importance of the scattering index screening which rejects about 32% of observations, whilst only 6-7% of observations are rejected by the additional quality controls. Figure 21 examines latitude and longitude location of SSMI/S channel 9 observations selected by the screening methodology. As a reference of cloudiness, the monthly mean total hydrometeor content is also shown. The observations selected by the screening methodology seem to be well globally distributed and, consistently, a small number of data is selected in areas with large hydrometeor amount, such as Central Africa, India, Thailand and Indonesia. The capability of the screening methodology is also confirmed by GOES and Meteosat images which observed cloud systems over the same regions.

Data from MHS sensors are operationally assimilated over land within the ECMWF system. Hence, they provide a reference to assess the approach proposed in this work. Figure 22 shows PDFs of SSMI/S (F17) and MHS (NOAA-18) humidity sounding channel first guess departures, where SSMI/S observations have been selected by the screening methodology, whilst MHS observations are those actively assimilated within the ECMWF system. The results are very promising: SSMI/S and MHS have very similar distribution of first guess departures in shape and intensity. To give a statistical measure of the two sets of observations, we can compare the standard deviation (STD) computed over the whole first guess departures sample channel by channel, as shown in table 6. In the same latitude range (-60,60) and observational time (1-31 August 2011), the SSMI/S data sample has STD similar to those computed over the actively assimilated MHS observation, with lower STD at channels 10 and 11. This trend, is also confirmed by two additional experiments run over 1-30 September and 1-31 October 2011.

Aside from confirming the consistency of the strategy implemented, the standard deviations computed over the whole SSMI/S first guess departures sample also provide a way to characterise an observation error to give to each channel. In fact, the further extension of this work is to implement active data assimilation within the ECMWF system. Hence, quantifying a plausible observation error is very important. Ignoring cross-correlations between errors in the observation and in the background, from the results of this study, it is reasonable to infer that the following observation errors might be assigned to the SSMI/S humidity sounding channels (channel 9, channel 10 and channel 11): 1.70, 1.70 and 1.80.

SSMI/S	STD (K)	OBS	MHS	STD (K)	OBS
channel 9	1.66	201011	channel 5	1.56	123409
channel 10	1.66	200245	channel 4	1.73	134924
channel 11	1.74	197850	channel 3	1.93	157652

Table 6: Standard deviation (STD) computed over the whole SSMI/S and MHS first guess departures sample of observations (OBS): for those OBS selected by the screening methodology, SSMI/S, and for those OBS actively assimilated within the ECMWF system, MHS. The sample of observations is from 1 to 31 August 2011 and latitude ranges from -60 to 60 degrees.

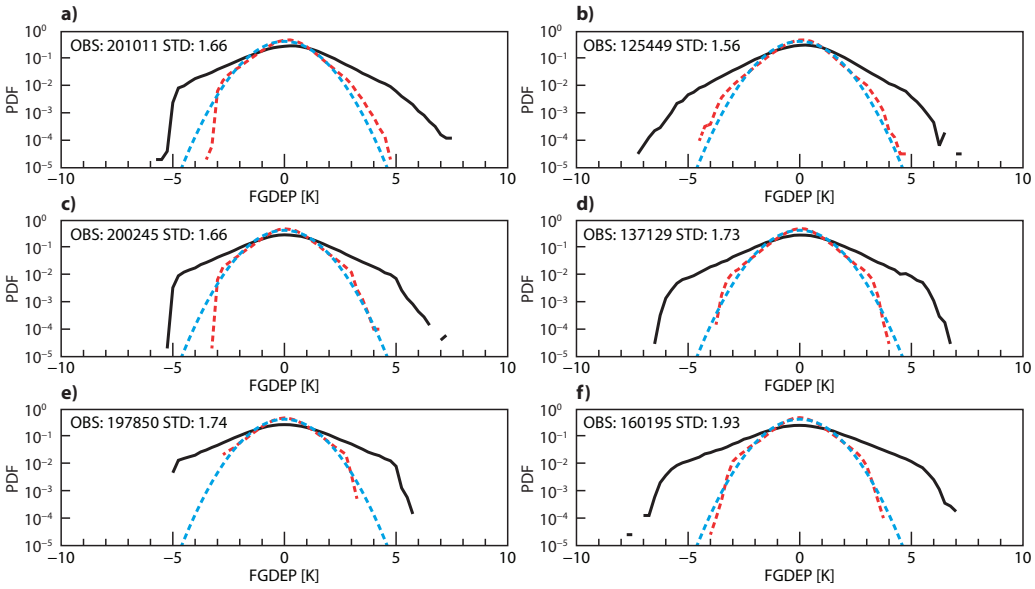

Figure 22: PDFs of SSMI/S and MHS humidity sounding channels first guess departures (black lines): SSMI/S channel 9 (183.31 $\pm$ 6.6), a, vs MHS channel 5 (183.0 $\pm$ 7.0), b, channel 10 (183.31 $\pm$ 3.0), c, vs channel 4 (183.0 $\pm$ 3.0), d, and channel 11 (183.31 $\pm$ 1.0), e, vs channel 3 (183.0 $\pm$ 1.0), f. SSMI/S: observations where land surface emissivities were retrieved from channel 18 (91h) and subsequently selected by the screening methodology; MHS: observations actively assimilated within the ECMWF system. Bin size is 0.25 K. The sample of observations is 1 month of data (1-31 August 2011) and latitude ranges from -60 to 60 degrees. The dotted red line gives the PDF normalised by the standard deviation of the whole sample, whilst the dotted blue line gives the Gaussian distribution as a reference. Number of observations (OBS) and standard deviation (STD) of the whole sample are also shown.

Finally, as additional verification, figures 23, 24 and 25 show mean first guess departure maps of SSMI/S humidity sounding channels for the initial set of data over land and for those observations selected by the screening methodology and, as reference, mean first guess departures maps of MHS channels for those observation actively assimilated within the ECMWF system. The large negative biases visible in different parts of the globe in the initial SSMI/S observation sample are completely removed. After the screening slight positive biases seem to appear in some central regions of Africa. However, it might be a sampling issue due to the low number of observations that end up in those bins (figure 21 as a reference). Analysing MHS mean first guess departures maps, we can appreciate the screening impact. Operationally, MHS observations are assimilated in a clear-sky scheme where the screening methodology rejects observations according to thresholds on model orography, surface temperature and channel 2 (150 GHz) first guess departures. Orography screening, which depends on the channel sensitivity, rejects observations over high orography (reject observations above 1500 m, channel 3, 1000 m, channel 4 and 800 m, channel 5). The impact of this screening can be easily noticed in different parts of the globe (Asia, Southern Africa and Northern America) where MHS observations are not assimilated. On the contrary, over the same regions, the screened SSMI/S observations do not appear to be affected by large biases.

Another interesting difference is for SSMI/S channel 11 and MHS channel 3. MHS observations seem to be affected by negative first guess departures over the northern part of south America. This might be explained by the presence of cirrus clouds and by the fact that channel at 183.3 ± 1.0 GHz is more sensitive to the top of the cloud having peak of sensitivity between 6000 and 8000 m. Images from GOES confirm that cloud systems were localised over the northern part of South America for many days during August 2011. This might be a deficiency in the MHS quality checks and actively assimilated observations might still be cloud-affected and, consequently, the clear-sky approach cannot resolve the biases properly. On the contrary, the residual cloud contamination, which the SSMI/S screening methodology might reasonably take into account, seems to be correctly managed by the all-sky framework.

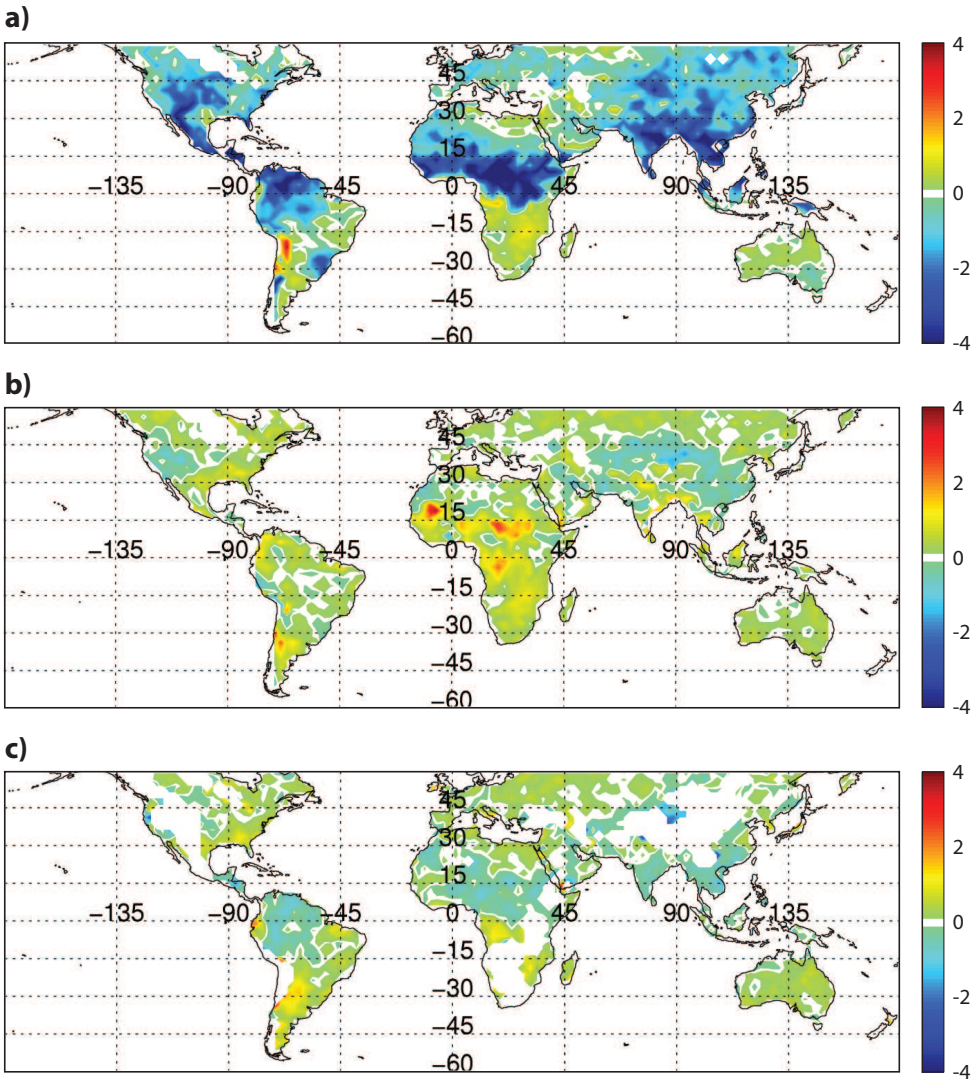

Figure 23: Mean first guess departures maps of SSMI/S channel 9 (183.31 ± 6.6): a, initial set of observations over land, where land surface emissivities were retrieved from channel 18 (91h); b, as in a, but where the screening methodology were applied, b. As a reference, c shows mean first guess departures of MHS channel 5 (183.0 ± 7.0) for those observations actively assimilated within the ECMWF system. Maps are binned in 2.5 by 2.5 boxes. The sample of observations is 1 month of data (1-31 August 2011)

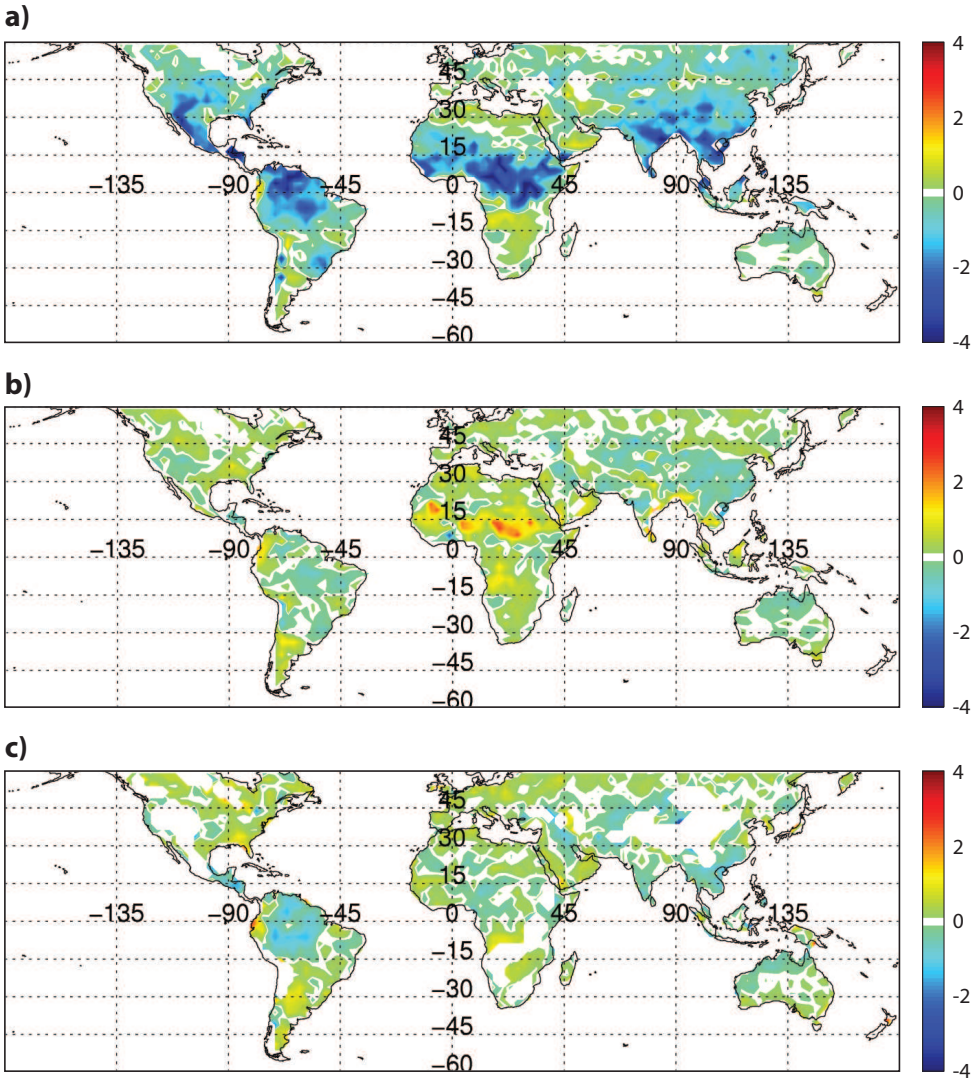

Figure 24: As figure 23, but for SSMI/S channel 10 (183.31 ± 3.0 GHz), a and b, and for MHS channel 4 (183.0 ± 3.0), c.

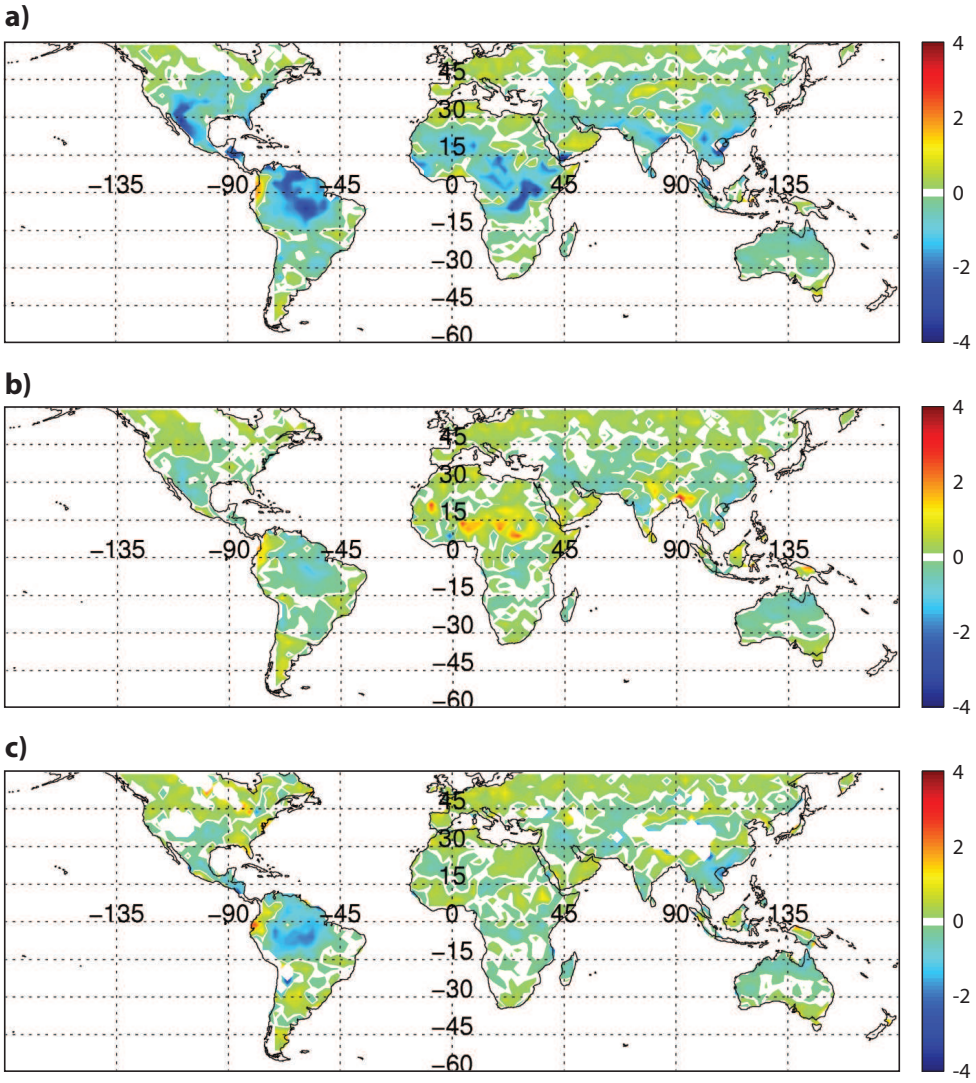

Figure 25: As figure 23, but for SSMI/S channel 11 (183.31 ± 1.0 GHz), a and b, and for MHS channel 3 (183.0 ± 1.0), c.

4 Summary and conclusions

This report summarises a feasibility study investigating the possibility to assimilate SSMI/S humidity sounding observations over land in the all-sky framework.

The first part of this investigation looked at the implementation and verification of emissivity retrievals within the all-sky framework. Being a parameter directly involved in the radiative transfer calculations, a reliable land surface emissivity estimation is the basic starting point in order to be able to consider land assimilation. The emissivity retrieval scheme was implemented so that it could be applied to any satellite observation available in the all-sky framework (TMI, SSMI/S or AMSU-A). It was coded within the scattering radiative transfer code (RTTOV-SCATT) in order to take into account cloud and precipitation. Emissivity estimates from TELSEM, a Tool to Estimate Land Surface Emissivities at Microwave frequencies, and AMSU-A clear-sky retrievals obtained by a completely independent path through the IFS code, were used as a reference to assess the retrieval implementation. SSMI/S and AMSU-A window channels emissivity retrievals in the all-sky framework were found in good agreement with those provided by TELSEM and AMSU-A clear-sky estimates, confirming the consistency of the scheme implemented. The results also confirm an important feature: at higher microwave frequencies, independently of the sensor, observation geometry and the scheme implemented (clear-sky or all-sky), the emissivity estimation is more affected by cloud contamination and consequently it leads to retrievals which are probably incorrect and must be rejected.

The second part of the study investigated which SSMI/S humidity sounding observations might be selected and be a potential part of the 4D-Var minimisation. SSMI/S F17 observations over land were passively introduced into the incremental 4D-Var ECMWF system to allow emissivity retrievals and calculations of differences between observations and simulated brightness temperatures (so-called first guess departures). Assimilation experiments at T255 horizontal resolution (78 km), from August to October 2011, were run. Land emissivity retrieved from SSMI/S channel 18 (91 GHz, horizontal polarization) were given to the humidity sounding channels and the resultant first guess departures were examined.

The initial sample of SSMI/S observations shows PDFs of humidity sounding channel first guess departures that are far from symmetric and Gaussian. Large positive and negative first guess departures are observed in all channels with negative values that can be larger than -40 K. Over a radiatively warm surface like land, scattering from solid hydrometeors is the dominant process at higher microwave frequencies, cooling the observed brightness temperatures. Our findings show that the Mie soft sphere approximation used to model the scattering properties of ice and snow, strongly depending on distribution, shape and density of the particles, is not accurate enough leading to warmer modelled radiances than observed. Hence, we investigated the optimal use of a scattering index (SI) in order to select observations unaffected by rain and ice hydrometeor scattering processes.

The use of the SI defined as the difference between SSMI/S channel 17 and channel 8 (91v - 150h) was the main screening methodology. Even though the observed SI is not a symmetric predictor (a symmetric predictor would be $[SI_{obs} + SI_{fg}]/2$), the quality control check is able to produce a reasonable unbiased and Gaussian distribution of first guess departures. The SI screening is good enough to correct the large negative first guess departures biases, whilst the positive biases are basically unaffected. The results might be different if radiative transfer calculations were more accurate. In the future, we will revisit this work using more appropriate ice single scattering properties to simulated observed brightness temperatures.

After the SI quality control check, PDFs of SSMI/S humidity sounding channel first guess departures

normalised by the standard deviation of the whole sample show slight positive and negative biases. In order to balance these residual inconsistency out, we introduced other two additional screenings: the resultant PDFs of first guess departures normalised by the standard deviation of the whole sample have very close Gaussian shape. However, the main result is the importance of the scattering index screening which rejects about 32% of observations, whilst only 6-7% of observations are rejected by the additional quality controls. From the initial sample of SSMI/S data over land, 330543 observations (1-31 August 2011), surface emissivity estimates and quality control checks allow to select a sub-set of observations for every humidity channel as follows: 201011 observations, for channel 9, 200245 for channel 10 and 197850 for channel 11. In addition, the observations selected by the screening methodology seem to be well distributed globally and, consistently, a small number of data is selected in areas with large monthly mean hydrometeor amount, such as Central Africa, India, Thailand and Indonesia. The capability of the screening methodology is also confirmed by GOES and Meteosat images which show cloud systems over the same regions.

The resultant SSMI/S PDFs of first guess departures were also compared to those provided by MHS (NOAA-18) observations actively assimilated within the ECMWF system. The results show that SSMI/S and MHS have very similar distribution of first guess departures in shape and intensity and the standard deviations computed over the whole first guess departures sample are also comparable. Ignoring cross-correlations between errors in the observation and in the background, from the first guess departures, it is reasonable to infer that the following observation errors might be assigned to the SSMI/S humidity sounding channels (channel 9, channel 10 and channel 11): 1.70, 1.70 and 1.80.

Finally, analysing SSMI/S and MHS mean first guess departures maps, we were also able to appreciate the screening impact. The orography screening implemented for MHS data rejects observations over Asia, Southern Africa and Northern America, whilst SSMI/S screening does not. Over the same regions, the screened SSMI/S observations do not appear to be affected by large biases. Moreover, MHS channel 3 observations seem to be affected by negative first guess departures over the northern part of south America and this could be explained by residual cloud-contamination that, on the contrary, the SSMI/S all-sky approach is able to detect and model.

To conclude, the emissivity retrieval implemented in the all-sky framework is a helpful tool to further analyse and check emissivity seasonal variations and provide inter-sensor comparisons. We will also investigate in more detail the impact of land surface emissivity retrieved by satellite observations within assimilation experiments. Work at ECMWF is currently ongoing to improve RTTOV-SCATT simulations and investigate the possibility to migrate from Mie sphere approximation to more appropriate shapes. This work will be again revisited in order to evaluate the impact of any other particle scattering model. Nonetheless, considering an optimal scattering index screening, SSMI/S humidity sounding observations might be assimilated over land in the all-sky framework. The SI quality check proposed in this report might also be investigated for assimilating observations in all-sky conditions over land from other microwave humidity sounding instruments, such as MHS and ATMS. In the future, we will implement and code this methodology within the ECMWF system. It is necessary to make a number of changes in the all-sky framework in order to allow land observations to be correctly selected and managed. This task has already commenced. As soon as the system is ready, assimilation experiments will be set up and run and it will be possible to check and evaluate the impact of SSMI/S humidity sounding channels in the ECMWF 4D-Var system. We intend to achieve these goals in the next year of the EUMETSAT fellowship.

Acknowledgements

Fabrizio Baordo is funded through the EUMETSAT fellowship programme. Rob Hine is gratefully acknowledged for his help editing the figures.

Acronyms

AMSR-E - Advanced Microwave Scanning Radiometer on EOS
AMSU-A - Advanced Microwave Sounding Unit A
ATMS - Advanced Technology Microwave Sounder
GOES - Geostationary Operational Environmental Satellite
IFS - Integrated Forecast System
MHS - Microwave Humidity Sounder
NOAA - National Oceanic and Atmospheric Administration
NESDIS - The National Environmental Satellite, Data, and Information Service
RTTOV - Radiative Transfer for TOVS
SSM/I - Special Sensor Microwave Imager
SSMI/S - Special Sensor Microwave Imager Sounder
TELSEM - Tool to Estimate Land Surface Emissivity at Microwave frequencies
TMI - TRMM Microwave Imager

References

Aires F., C. Prigent, F. Bernado, C. Jimnez, R. Saunders, P. Brunel, 2010. A tool to estimate Land Surface-Emissivities at Microwaves frequencies (TELSEM) for use in numerical weather prediction. Q. J. R. Meteorol. Soc. 137, 690−699.

Bauer P., Moreau E., Chevallier F., OKeeffe U., 2006. Multiple-scattering microwave radiative transfer for data assimilation applications. Q. J. R. Meteorol. Soc. 132, 1259−1281.

Bauer P, Geer A. J., Lopez P, Salmond D., 2010. Direct 4D-Var assimilation of all-sky radiances. Part I: Implementation. Q. J. R. Meteorol. Soc. 136, 1868−1885.

Bell, W., English, S.J., Candy, B., Atkinson, N., Hilton, F., Baker, N., Swadley S.D., Campbell, W.F., Bormann, N., Kelly, G., Kazumori, M., 2008. The assimilation of SSMIS radiances in numerical weather prediction models. IEEE Transactions on Geoscience and Remote Sensing, v.46, p.884−900.

Bennartz, Thoss, Dybbroe and Michelson, 2002. Precipitation analysis using the Advanced Microwave Souunding Unit in support of nowcasting applications. Meteorol. Appl., 9, 177−189.

Bennartz, R., Bauer, P., 2003. Sensitivity of microwave radiances at 85−183 GHz to precipitating ice particles. Radio Sci. 38, 8075.

Doherty, A. M., Sreerekha T. R., OKeeffe, U., English S. J., 2007. Ice hydrometeor microphysical assumptions in radiative transfer models at AMSU-B frequencies. Q. J. R. Meteorol. Soc. 133, 1205−1212.

English S. J., and Hewison T. J., 1998. A fast generic millimeter-wave emissivity model. Microwave

Remote Sensing of the Atmosphere and Environment, T. Hayasaka et al., Eds., International Society for Optical Engineering (SPIE Proceedings), 3503, 288−300.

Evans, K.F., Stephens, G.L., 1995. Microwave radiative transfer through clouds composed of realistically shaped ice crystals. Part I: Single scattering properties. J. Atmos. Sci. 52, 2041−2057.

Evans, K.F., Stephens, G.L., 1995a. Microwave radiative transfer through clouds composed of realistically shaped ice crystals. Part II: Remote sensing of ice clouds. J. Atmos. Sci. 52, 2058−2072.

Ferraro, R. R., and G. F. Marks, 1995. The development SSM/I rain rate of retrieval algorithms using ground based radar measurements. J. Atmos. Oceanic Technol., 12, 755−770.

Geer A. J., Bauer, P., C. W. ODell., 2009. A revised cloud overlap scheme for fast microwave radiative transfer in rain and cloud. J. Applied Meteorology, 48, 2257−2270.

Geer A. J., Bauer P., Lopez P., 2010. Direct 4D-Var assimilation of all-sky radiances: Part II. Assessment. Q. J. R. Meteorol. Soc. 136, 1886−1905.

Geer A. J., and Bauer P., 2011. Observation errors in all-sky data assimilation. Q.J.R. Meteorol. Soc. 137: 2024−2037.

Geer, A. J., Bauer P., S. J. English, 2012. Assimilating AMSU-A temperature sounding channels in the presence of cloud and precipitation, ECMWF (available from www.ecmwf.int/publications).

Grody, N. C., 1991. Classification of Snow Cover and Precipitation Using the Special Sensor Microwave Imager. Journal of Geophysical Research-Atmospheres, 96, 7423−7435.

Karbou F., Prigent C., Eymard L., Pardo J., 2005. Microwave land emissivity calculations using AMSU-A and AMSU-B measurements, IEEE Trans. on Geoscience and Remote Sensing, 46, 863−883.

Karbou F., Bormann N., Thpaut J-N, 2007. Towards the assimilation of satellite microwave observations over land: feasibility studies using SSMI/S, AMSU-A and AMSU-B, NWPSAF Tech. Rep., 37pp.

Krzeminski, B., Bormann N., Karbou F., Bauer P., 2009. Improved use of surface-sensitive microwave radiances over land at ECMWF. In Proceedings of the 2009 EUMETSAT Meteorological Satellite Conference, EUMETSAT, Darmstadt, Germany.

Kunkee, D.B., Poe, G.A., Boucher, D.J., Swadley, S.D., Hong, Ye., Wessel, J.E., Uliana, E.A., 2008. Design and evaluation of the first Special Sensor Microwave Imager/Sounder, IEEE Trans. on Geoscience and Remote Sensing, 43, 5, 948−959.

Liu, G., 2004. Approximation of single scattering properties of ice and snow particles for high microwave frequencies. J. Atmos. Sci. 61, 2441−2456.

Prigent C., Rossow W. B., Matthews E., 1997. Microwave land surface emissivities estimated from SSM/I observations, J. Geophys. Res., 102, 21867−21890.

Prigent C., Chevallier F., Karbou F., Bauer P., Kelly G., 2005. AMSU-A surface emissivities for numerical weather prediction assimilation schemes, J. Applied Meteorology, 44, 416−426.

RTTOV v10, Users guide v1.5, available from http://research.metoffice.gov.uk/research/interproj/nwpsaf/rtm

Sun, N., F. Weng. 2008. Evaluation of Special Sensor Microwave Imager/Sounder (SSMI/S) Environmental Data Records. IEEE Transactions on Geoscience and Remote Sensing. 46, no. 4.